Non-coherent Cell-free Large SIMO using DMPSK

Lopez Morales, Manuel Jose; Chen Hu, Kun; Alvarez Polegre, Alberto; García Armada, Ana

Published in:
IEEE Transactions on Vehicular Technology

DOI (link to publication from Publisher):
10.1109/TVT.2023.3332821

Publication date:
2024

Document Version
Accepted author manuscript, peer reviewed version

Non-coherent Cell-free Large SIMO using DMPSK

Manuel J. Lopez-Morales, *Graduate Student Member, IEEE*, Kun Chen-Hu, *Member, IEEE*, Alberto Alvarez-Polegre, *Member, IEEE*, Ana Garcia-Armada, *Senior Member, IEEE*

***Abstract*—A cell-free non-coherent (NC) massive single-input-multiple-output (SIMO) system is proposed in a wireless uplink where a single-antenna user transmits to several multi-antenna access points (APs). NC detection using differential phase shift keying is the utilized detection technique in this system. It has the advantage that no channel state information (CSI) is required in the APs for signal reception, so it is beneficial with respect to coherent massive MIMO in stringent scenarios where channel state information has very low quality. Additionally, it outperforms the single-AP NC massive SIMO due to the increased number of antennas to average the received signal. The distribution of the received symbol of the NC multi-AP processing is analytically derived to show that several geographically distributed antennas result in a distribution with smaller variances. Several AP selection techniques to maximize the performance and minimize the complexity of the scheme are also proposed. Numerical results are provided to demonstrate the validity of the analysis and to show that the proposal outperforms both the coherent CF schemes in scenarios with stringent conditions and the single-AP NC massive SIMO.**

***Index Terms*—Non-coherent, massive SIMO, differential modulation, cell-free, AP selection.**

I. Introduction

In the last years, wireless networks have seen tremendous developments to accommodate the technical requirements of several emerging innovative applications, such as 4K/8K video streaming, virtual/augmented reality, cloud gaming, real-time remote control and autonomous driving, among others. 5G is already under deployment to manage some of these needs [1], but its capabilities will not be sufficient for the most demanding foreseen applications [2]. In this context, extensions beyond 5G and the future 6G will be developed to cope with the ever-increasing demands of future wireless networks. Higher data rates, lower latency, higher reliability, a greater number of connected devices and lower energy consumption are requirements for future networks, while scenarios such as fast varying channels and/or low signal-to-noise ratios are envisioned with vehicular and aerial communications taking remarkable importance [2].

An interesting technology to increase the spectral and energy efficiency is massive single-input multiple-output (mSIMO) in the uplink (UL) and massive multiple-input single-output (mMISO) in the downlink (DL) of a user [3], which consists of placing large antenna arrays in the access point (AP), either to increase the cell sum data-rate by multiplexing different streams or to provide higher robustness through spatial diversity. Typically, classical coherent communications are applied in mSIMO, which are based on estimating the channel and pre/post-coding the data to compensate for the effects introduced by the propagation channel in the communication signals, so that the data can be effectively detected in the receiver. In order to acquire the so-called channel state information (CSI), reference signals are required. For some stringent scenarios such as fast varying channels (short coherence bandwidth and time) and/or low signal-to-interference-plus-noise ratio (SINR), the CSI acquisition greatly limits the efficiency of coherent systems [4], since too many pilot signals are required, either to effectively track the channel variations or to estimate the channel with sufficient quality. In fact, in these scenarios, the classical coherent scheme does not work even for one user if this user moves very fast or if it has a very low SINR [4]. Blind channel estimation techniques permit to acquire CSI without using pilot reference signals, but they are strongly limited in those channels with a short coherence bandwidth and time [5]. Alternatively, to blind channel estimation, non-coherent (NC) schemes based on differential M-ary phase shift keying (DMPSK) arise as an interesting technique capable of obtaining the transmitted data without the need to acquire any CSI [6]–[10], which only needs enough channel correlation in two consecutive symbols, either in time or frequency domains [7]. On the contrary, coherent schemes need to transmit reference signals to acquire channel knowledge and pre/post-compensate the channel effects. Particularly channel aging, low SINR during channel estimation, and pilot contamination could lead to an erroneous CSI acquisition in coherent techniques, which is not the case for systems based on NC communication. Please note that the term NC used in this manuscript refers to the classical meaning of detecting data in a mSIMO uplink without utilizing any CSI. It does not mean that APs are sending different data, as in [11].

Both coherent and NC schemes experience performance degradation in spatially correlated channels [12], even though NC schemes have been proven to be more robust than coherent ones to these effects [13]. This kind of channel is typical in mSIMO deployments. The spatial correlation in the AP is caused by the antenna coupling, the antenna array geometry and the clustered propagation channel [3], [14], [15]. Besides this, it was shown in [12] that the NC scheme can benefit from receiving the signal in a set of geographically distributed and coordinated APs since their channels are nearly

This work has received funding from the European Union (EU) Horizon 2020 research and innovation programme under the Marie Skłodowska-Curie ETN TeamUp5G, grant agreement No. 813391, and from the Spanish National Project IRENE-EARTH (PID2020-115323RB-C33/AEI/10.13039/501100011033, UE).

Manuel J. Lopez-Morales and Ana Garcia-Armada are with the Department of Signal Theory and Communications, Universidad Carlos III de Madrid, Spain. Email: {mjlopez,agarcia}@tsc.uc3m.es.

Kun Chen-Hu is with the Department of Signal Theory and Communications, Universidad Carlos III de Madrid, Spain, and the Department of Electronic Systems, Aalborg University, Denmark. Email: kchenhu@es.aau.dk.

Alberto Alvarez-Polegre is with The MathWorks SL, Madrid, Spain. Email: aalvarez@mathworks.com.

uncorrelated and then, the problem of spatial correlation is overcome. Furthermore, being able to receive the signal in several coordinated APs results in larger virtual antenna arrays, which will necessarily outperform the single-cell massive SIMO (SC-mSIMO). Cell-free massive SIMO (CF-mSIMO) is a technology currently proposed for coherent schemes in which a set of geographically distributed APs serve the users in the same time-frequency resource [16]. It can be seen as an evolution of the user-centric coordinated multipoint joint-transmission (CoMP-JT) [17]. By making a user-centric access approach and abandoning the paradigm of cell-based communication networks, CF-mSIMO benefits from the fact that there is a very low correlation between the channels seen at different APs [18]. In contrast, the performance of coherent CF-mSIMO will be limited, as previously mentioned for SC-mSIMO, in scenarios of fast varying channels and/or low SNR for the same previously-mentioned reasons.

In this paper we propose to apply the NC approach in combination with a multi AP processing for the UL of a mSIMO, to overcome the limitations inherent to NC processing caused by spatially correlated channels. Our proposal, named non-coherent cell-free (NC-CF), can outperform both the classical cell-free (CF) coherent processing and the single-AP non-coherent processing. The former is outperformed in fast varying and/or low signal-to-noise ratio (SNR) channels due to the fact that its performance depends directly on the CSI quality. The latter is outperformed since the NC-CF will potentially receive more signals through spatially uncorrelated channels, which will improve the performance of NC processing by means of averaging. The proposed scheme is based on applying non-coherent massive SIMO (NC-mSIMO) processing using DMPSK [4], [6] in a CF-mSIMO [18] deployment. The contributions are summarized below:

- A NC approach is combined with multi-AP processing for the UL of a mSIMO and proposed as a novel scheme capable of outperforming both the equivalent coherent CF and the single-cell NC scheme.
- To show the benefit of the proposed system, a symbol error rate (SER) analysis of the NC scheme in a multi-AP scenario is provided. The probability density function (PDF) of the received signal in the NC-mSIMO system based on DMPSK is provided for an antenna element, for an AP and for a multi-AP scenario with spatially correlated Rician fading channels. To the best of the authors' knowledge, these analyses are not available in the literature. The analysis shows that the NC scheme benefits from the line-of-sight (LoS) component of the Rician channel, suffers when the spatial correlation is large and benefits when several uncorrelated APs are coordinated.
- Given a scenario of multiple APs, a set of strategies of AP selection are given. Namely, brute-force search, successive and smart successive selection, are proposed to coordinate multiple APs and improve the overall performance when applying a NC approach. Besides, the different strategies are also evaluated in terms of complexity. Each AP selection technique has a trade-off and depending on the available computing capabilities and the required quality-of-service (QoS), it is up to the developer to select which selection technique to use.
- A comparison in terms of performance and complexity is made between the coherent and the NC-CF schemes, to justify that the NC-CF approach performs better than the coherent counterpart in the above-mentioned scenarios.
- The proposed techniques are validated with numerical results. We first show via Monte Carlo simulations that the bit-error-rate (BER) and SINR analyses are accurate. Secondly, we show the performance and the complexity of the AP selection strategies for the NC-CF. Lastly, we show a comparison in terms of performance and complexity of the coherent and the NC-CF schemes and demonstrate the NC is a better option in some scenarios of interest.

The remainder of the paper is organized as follows. Section II provides the channel and system model for the proposed NC-CF massive SIMO (NC-CF-mSIMO); Section III provides a BER and SINR analysis of the NC-CF-mSIMO; Section IV introduces the NC-CF-mSIMO AP selection strategies with their complexity; Section V compares the coherent CF and the NC-CF approaches; Section VI shows some numerical results; and Section VII concludes the paper.

Notation: matrices, vectors and scalar quantities are denoted by boldface uppercase, boldface lowercase, and regular lowercase letters, respectively. $[\mathbf{A}]_{m,n}$ denotes the element in the m-th row and n-th column of $\mathbf{A}$. $[\mathbf{a}]_n$ represents the n-th element of vector $\mathbf{a}$. $\angle(x)$ and $\lceil x \rceil$ represent the angle and closest superior integer number of x, respectively. The superscripts $(\cdot)^H$, $(\cdot)^*$ and $(\cdot)^\dagger$ denote Hermitian, complex conjugate and Moore-Penrose pseudoinverse, respectively. $\mathbb{E}\{\cdot\}$ represents the expected value. $\mathrm{Var}\{\cdot\}$ denotes variance. $\mathcal{CN}(0,\sigma^2)$ represents the circularly-symmetric and zero-mean complex normal distribution with variance σ^2 and $U(a,b)$ represents the uniform distribution between a and b. $f(a|b)$ and $P(a|b)$ is the conditional probability density function (PDF) of a conditioned to b for continuous and discrete random variables, respectively. $\Gamma(k,\xi)$ is the Gamma distribution with shape parameter k and scale parameter ξ, with mean $\mu = k/\xi$ and variance $\sigma = k/\xi^2$. $\Re$ and $\Im$ refer, respectively, to the real and imaginary parts of a complex number. $||x||_2$ denotes the euclidean norm of x. $\mathbf{1}$ and $\mathbf{0}$ indicate a column vector of all ones and all zeros, respectively. $Q(\cdot)$ indicates the Q-function.

II. System model

We consider a generic mSIMO system with A APs, with R_a antennas in AP a, and we focus on a particular user with one antenna. In the case of cooperation, it is assumed that the APs are connected to a central processing unit (CPU) by means of fronthaul links, whose constraints are not taken into account. It is assumed that the channel coherence time is defined as τ_c.

A. Channel Model

The propagation channel between the user and the AP a at time instant n is represented by $\mathbf{h}_a^n$ $(R_a \times 1)$. In detail,

$$\mathbf{h}_a^n = \sqrt{\alpha_a^n}\left(\bar{\mathbf{h}}_a^n + \mathbf{g}_a^n\right), \tag{1}$$

where α_a^n denotes the channel gain accounting for path loss and shadow fading (large-scale fading), $\bar{\mathbf{h}}_a^n$ ($R_a \times 1$) represents a line-of-sight (LoS) component, where all elements are equal to $|\bar{h}_a^n| e^{j\theta_a^n}$, so that $\mathbf{h}_a^n \sim \mathcal{CN}\left(\sqrt{\alpha_a^n}\bar{\mathbf{h}}_a^n, \alpha_a^n(\sigma_{h,a}^n)^2\mathbf{R}_a^n\right)$ and $\theta_a^n \sim U(0, 2\pi)$,

$$|\bar{h}_a^n|^2 = \frac{K_a^n}{K_a^n+1},\ (\sigma_{h,a}^n)^2 = \frac{1}{K_a^n+1} \text{ and } (\sigma_{h,a}^n)^2 + |\bar{h}_a^n|^2 = 1, \tag{2}$$

where K_a^n is the Rician factor, which characterizes the fading model and $\mathbf{g}_a^n$ ($R_a \times 1$), with $\mathbb{E}\left\{(\mathbf{g}_a^n)(\mathbf{g}_a^n)^H\right\} = (\sigma_{h,a}^n)^2\mathbf{R}_a^n$ ($\mathbf{R}_a^n$ is a normalized Hermitian matrix of size ($R_a \times R_a$)), which represents spatial correlation effects of small-scale fading, i.e. the non-line-of-sight (NLoS) component. We assume that the channel in two consecutive symbol time instants can be regarded approximately equal, $[\mathbf{h}_a^{n-1}]_{r_a} \approx [\mathbf{h}_a^n]_{r_a}$, for any antenna, where $1 \le r_a \le R_a$ refers to the antenna r_a in AP a. The channel coefficients between APs are uncorrelated as $\mathbb{E}\left\{(\mathbf{h}_a^n)(\mathbf{h}_{a'}^n)^H\right\} = \mathbf{0} \quad \forall a \neq a'$.

B. Proposed non-coherent cell-free massive SIMO

We propose a NC-CF-mSIMO in which the channel estimation is avoided since it is not needed to detect the transmitted data. Therefore, this proposal is not affected by the limitations inherent to the channel estimation. Besides this, the NC system will benefit from multi-AP processing due to the fact that the spatial correlation is reduced between APs and a higher number of effective antennas are utilized.

We focus on the particular case of the UL, where the user transmits a differentially encoded signal at time instant n

$$x^n = x^{n-1}s^n \quad 1 \le n \le N, \tag{3}$$

where s^n is the symbol belonging to a DMPSK constellation and x^0 is a reference symbol known at the receiver side and necessary to perform the differential reception. Because the information is only encoded in the phase, we know that $(x^{n-1})^* x^n = s^n$.

The received signal at AP a and n-th time instant is

$$\mathbf{y}_a^n = \mathbf{h}_a^n x^n + \boldsymbol{\nu}_a^n, \tag{4}$$

where x^n denotes the transmitted symbol at time n by the user of interest and $\boldsymbol{\nu}_a^n$ ($R_a \times 1$) represents the additive white Gaussian noise according to $\boldsymbol{\nu}_a^n \sim \mathcal{CN}(\mathbf{0}, (\sigma_{\nu,a}^n)^2\mathbf{I}_{R_a})$. Finally, the average SNR in AP a is defined as $\rho_a = \alpha_a^n(\sigma_{\nu,a}^n)^{-2}$, where the power of the transmitted symbols is normalized to one and the channel effects are not taken into account since they average out.

In reception at each AP a, two contiguous differential symbols in the time domain are non-coherently combined as

$$z_a^n = (\mathbf{y}_a^{n-1})^H \mathbf{y}_a^n = \sum_{r_a=1}^{R_a} \left[\mathbf{y}_a^{n-1}\right]_{r_a}^* \left[\mathbf{y}_a^n\right]_{r_a} = \sum_{r_a=1}^{R_a} \left[\mathbf{z}_a^n\right]_{r_a}, \tag{5}$$

where $\left[\mathbf{z}_a^n\right]_{r_a} = \left[\left[\mathbf{y}_a^{n-1}\right]_1^* \left[\mathbf{y}_a^n\right]_1, \cdots, \left[\mathbf{y}_a^{n-1}\right]_{R_a}^* \left[\mathbf{y}_a^n\right]_{R_a}\right]^T$.

In a scenario with $A > 1$ APs (multi-AP), some selected variables z_a are sent to the CPU and combined as

$$z^n = \frac{\sum_{a\in\mathcal{A}_s} z_a^n}{\sum_{a\in\mathcal{A}_s} R_a}, \tag{6}$$

where $\mathcal{A}_s$ indicates the subset of APs selected to send their z_a^n to the CPU for decision and z^n is the variable over which the transmitted symbols are estimated according to [6] as

$$\hat{s}^n = \arg\min_{s^n} \{|s^n - z^n|,\ s^n \in \mathfrak{M}\}, \tag{7}$$

where $\mathfrak{M}$ indicates the DMPSK constellation set with M elements. The proposed detection process in (6) is made by first performing a distributed processing in each AP following (5) and then the resulting variable z_a^n in each AP is sent to the CPU for a centralized combining. This is proposed, rather than sending the raw data to the CPU and performing detection as in [6], since the result is mathematically the same while the fronthaul would be unnecessarily overloaded. A mean SNR for the APs is defined as

$$\bar{\rho} = \frac{1}{A}\sum_{a=1}^{A}\rho_a = \frac{1}{A}\sum_{a=1}^{A}\frac{\alpha_a^n}{(\sigma_{\nu,a}^n)^2}. \tag{8}$$

It is worth noting that our proposal does not need to estimate the channel as it is the case for the coherent scheme, which is explained in Section V. Therefore, this proposal is more efficient in terms of throughput and complexity.

III. Distortion, Interference and Noise Terms in Non-coherent Cell-free M-DPSK Massive SIMO

The distortion, interference and noise (DIN) terms in each AP a is obtained in this section since it will be useful to characterize the performance of each post-processing scheme proposed in Section IV. To account for the case of APs with $R_a = 1$, we have to analyze first the distribution per antenna, later per AP and last for several APs. Mathematical preliminaries that are useful to understand this section can be found in Appendix B. The distribution of the received symbol $\left[\mathbf{z}_a^n\right]_{r_a}$ is given in [19]. However, it is shown as an approximation which is not rigorously justified by means of a mathematical demonstration or a reference. Furthermore, the noise term is considered negligible, which can be done only in the high SNR scenario. Due to the fact that the work in this manuscript is intended for low SNR scenarios (among others), we cannot use such an approximation. Therefore, we compute the exact distribution of the received symbol at each antenna element, at each AP and for the multi-AP processing.

A. Distribution of the received symbol $\left[\mathbf{z}_a^n\right]_{r_a}$

Taking into account that the product of a circularly symmetric variable by x^n or $(x^n)^*$ does not change the variable distribution and with some straightforward derivations, (5) can be expanded as

$$\begin{aligned}\left[\mathbf{z}_a^n\right]_{r_a} = &\underbrace{\left[\mathbf{h}_a^{n-1}\right]_{r_a}^* \left[\mathbf{h}_a^n\right]_{r_a}}_{[\mathbf{z}_a^n]_{r_a}^{(1)}} \underbrace{(x^{n-1})^* x^n}_{s^n} + \underbrace{\left[\boldsymbol{\nu}_a^{n-1}\right]_{r_a}^* \left[\boldsymbol{\nu}_a^n\right]_{r_a}}_{[\mathbf{z}_a^n]_{r_a}^{(2)}} + \\ &+ \underbrace{\left[\boldsymbol{\nu}_a^{n-1}\right]_{r_a}^* \left[\mathbf{h}_a^n\right]_{r_a}}_{[\mathbf{z}_a^n]_{r_a}^{(3)}} x^n + \underbrace{\left[\mathbf{h}_a^{n-1}\right]_{r_a}^* \left[\boldsymbol{\nu}_a^n\right]_{r_a}}_{[\mathbf{z}_a^n]_{r_a}^{(4)}} (x^{n-1})^*,\end{aligned} \tag{9}$$

where (and since $[\mathbf{g}_a^n]_{r_a} \approx [\mathbf{g}_a^{n-1}]_{r_a}$ and $[\bar{\mathbf{h}}_a^n]_{r_a} \approx [\bar{\mathbf{h}}_a^{n-1}]_{r_a}$) each element expands as

$$\begin{aligned}\left[\mathbf{z}_a^n\right]_{r_a}^{(1)} &= \alpha_a^n \left([\bar{\mathbf{h}}_a^n]_{r_a}^* + [\mathbf{g}_a^n]_{r_a}^*\right)\left([\bar{\mathbf{h}}_a^n]_{r_a} + [\mathbf{g}_a^n]_{r_a}\right) = \\ &= \alpha_a^n |\bar{h}_a^n|^2 + \underbrace{2\alpha_a^n \Re\{[\bar{\mathbf{h}}_a^n]_{r_a}^* [\mathbf{g}_a^n]_{r_a}\}}_{[\mathbf{z}_a^n]_{r_a}^{(1,1)}} + \underbrace{\alpha_a^n \left|[\mathbf{g}_a^n]_{r_a}\right|^2}_{[\mathbf{z}_a^n]_{r_a}^{(1,2)}},\end{aligned} \tag{10}$$

$$\left[\mathbf{z}_a^n\right]_{r_a}^{(3)} = \underbrace{\sqrt{\alpha_a^n}[\boldsymbol{\nu}_a^n]_{r_a}^* [\bar{\mathbf{h}}_a^n]_{r_a}}_{[\mathbf{z}_a^n]_{r_a}^{(3,1)}} + \underbrace{\sqrt{\alpha_a^n}[\boldsymbol{\nu}_a^n]_{r_a}^* [\mathbf{g}_a^n]_{r_a}}_{[\mathbf{z}_a^n]_{r_a}^{(3,2)}}, \tag{11}$$

$$\left[\mathbf{z}_a^n\right]_{r_a}^{(4)} = \underbrace{\sqrt{\alpha_a^n}[\bar{\mathbf{h}}_a^n]_{r_a}^* [\boldsymbol{\nu}_a^n]_{r_a}}_{[\mathbf{z}_a^n]_{r_a}^{(4,1)}} + \underbrace{\sqrt{\alpha_a^n}[\mathbf{g}_a^n]_{r_a}^* [\boldsymbol{\nu}_a^n]_{r_a}}_{[\mathbf{z}_a^n]_{r_a}^{(4,2)}}. \tag{12}$$

From now on, we drop the superscript "n" for ease of reading. The distributions of eqs. (10)-(12) are shown in Appendix C.

B. Distribution of the received symbol z_a at each AP

We calculate the distribution of the real part and the imaginary part separately since they will be different due to the differential data detection [20]. Following the properties of variance Gamma (VG) distributions [21]–[23] and mathematical derivations of the sum and product of complex numbers, we can give a closed for expression of the distribution of the real and imaginary parts of the received symbol z_a at each AP, as shown in Appendix A.

Grouping the elements (53)-(56) of Appendix A via straightforward manipulations, the distribution of the received symbol (5) for APs with R_a antennas and spatial correlation defined by matrix $\mathbf{R}_a$ can be computed assuming $s = 1$ without loss of generality, as $\Re\{z_a\} \sim \mathcal{N}\left(\mu_{\Re\{z_a\}}, \sigma^2_{\Re\{z_a\}}\right)$ with

$$\mu_{\Re\{z_a\}} = R_a \alpha_a \left(\sigma^2_{h,a} + |\bar{h}_a|^2\right) = R_a \alpha_a, \tag{13}$$

$$\begin{aligned}\sigma^2_{\Re\{z_a\}} = \alpha_a^2 \sigma^2_{h,a} \left(\sigma^2_{h,a} ||\mathbf{R}_a||_2^2 + 2|\bar{h}_a|^2 \mathbf{1}^T \mathbf{R}_a \mathbf{1}\right) + \\ + 2^{-1} R_a \left(2\alpha_a \sigma^2_{\nu,a} + \sigma^4_{\nu,a}\right),\end{aligned} \tag{14}$$

and $\Im\{z_a\} \sim \mathcal{N}\left(\mu_{\Im\{z_a\}}, \sigma^2_{\Im\{z_a\}}\right)$ with

$$\mu_{\Im\{z_a\}} = 0, \quad \text{and} \quad \sigma^2_{\Im\{z_a\}} = \frac{R_a(2\alpha_a \sigma^2_{\nu,a} + \sigma^4_{\nu,a})}{2}. \tag{15}$$

The first term of (14) only depends on the propagation channel characteristics and the second term is equal to $\sigma^2_{\Im\{z_a\}}$, which depends on the path loss and the noise.

C. Distribution of the received symbol z in the CPU

Recalling (6), the distribution of z can be computed as the summation of several normally distributed random variables z_a [20] as $\Re\{z\} \sim \mathcal{N}\left(\mu_\Re, \sigma^2_\Re\right)$ with

$$\mu_\Re = \frac{\sum_{a\in\mathcal{A}_s} R_a \alpha_a}{\sum_{a\in\mathcal{A}_s} R_a}, \text{ and } \sigma^2_\Re = \frac{\sum_{a\in\mathcal{A}_s} \sigma^2_{\Re\{z_a\}}}{\left(\sum_{a\in\mathcal{A}_s} R_a\right)^2}, \tag{16}$$

and $\Im\{z\} \sim \mathcal{N}\left(\mu_\Im, \sigma^2_\Im\right)$ with

$$\mu_\Im = 0, \quad \text{and} \quad \sigma^2_\Im = \frac{\sum_{a\in\mathcal{A}_s} R_a(\sigma_a^4 + 2\alpha_{n,a}\sigma^2_{\nu,a})}{2\left(\sum_{a\in\mathcal{A}_s} R_a\right)^2}. \tag{17}$$

D. Special case of base stations with $R_a = 1,\ \forall a \in \mathcal{A}_s$

This is an interesting case to show that the law of large numbers still applies when sufficient APs are considered. Applying the properties of VG and Gamma distributions [21]–[23], for eqs. (47)-(51) and summing for $R_a = 1,\ \forall a$ for large number of A APs, we have

$$\sum_{a=1}^{A} \Re, \Im\left\{[\mathbf{z}_a]_1^{(3,2)} + [\mathbf{z}_a]_1^{(4,2)}\right\} \overset{A\to\infty}{\sim} \mathcal{N}\left(0, \sum_{a=1}^{A} \frac{\alpha_a \sigma^2_{h,a}}{\sigma^{-2}_{\nu,a}}\right), \tag{18}$$

$$\sum_{a=1}^{A} \Re, \Im\left\{[\mathbf{z}_a]_1^{(2)}\right\} \overset{A\to\infty}{\sim} \mathcal{N}\left(0, \sum_{a=1}^{A} \frac{\sigma^4_{\nu,a}}{2}\right), \tag{19}$$

$$\sum_{a=1}^{A} \Re, \Im\left\{[\mathbf{z}_a]_1^{(3,1)} + [\mathbf{z}_a]_1^{(4,1)}\right\} \overset{A\to\infty}{\sim} \mathcal{N}\left(0, \sum_{a=1}^{A} \alpha_a |\bar{h}_a|^2 \sigma^2_{\nu,a}\right), \tag{20}$$

$$\sum_{a=1}^{A} \Re\left\{[\mathbf{z}_a]_1^{(1,1)}\right\} \overset{A\to\infty}{\sim} \mathcal{N}\left(0, \sum_{a=1}^{A} 2\alpha_a^2 |\bar{h}_a|^2 \sigma^2_{h,a}\right), \tag{21}$$

$$\sum_{a=1}^{A} \Re\left\{[\mathbf{z}_a]_1^{(1,2)}\right\} \overset{A\to\infty}{\sim} \mathcal{N}\left(\sum_{a=1}^{A} \alpha_a \sigma^2_{h,a}, \sum_{a=1}^{A} \alpha_a^2 \sigma^4_{h,a}\right). \tag{22}$$

We obtain (22) using the condition $(\sum_a \alpha_a \sigma^2_{h,a})^3 >> (\sum_a \alpha_a^2 \sigma^4_{h,a})^2$, which is valid since $\alpha_a \sigma^2_{h,a} > \alpha_a^2 \sigma^4_{h,a}$ is always true and $\alpha_a, \sigma_{h,a} \in [0, 1]$ (due to the fact that the path loss can never be larger than 1 and $\sigma_{h,a} \leq 1$ by definition). To summarize and to simplify, in case that AP a has only one antenna, the distribution of z_a is the same as the one defined with eqs. (13), (14) and (15), particularizing with $||\mathbf{R}_a||_2^2 = \mathbf{1}^T \mathbf{R}_a \mathbf{1} = 1$. Thus, the distribution of z for $R_a = 1$ is valid using eqs. (16) and (17).

E. Special case when compensating path loss in each AP

In case the pathloss α_a is compensated in each AP locally before sending the data to the CPU, the signal in each AP would be defined as $\hat{z}_a = z_a/\alpha_a$, and the corresponding mean and variance would be $\mu_{\Re\{\hat{z}_a\}} = R_a$, $\sigma^2_{\Re\{\hat{z}_a\}} = \sigma^2_{\Re\{z_a\}}/\alpha_a^2$, $\mu_{\Im\{\hat{z}_a\}} = 0$ and $\sigma^2_{\Im\{\hat{z}_a\}} = \sigma^2_{\Im\{z_a\}}/\alpha_a^2$.

Thus, the centralized signal would be defined as $\hat{z} = \sum_{a\in\mathcal{A}_s} \hat{z}_a / \sum_{a\in\mathcal{A}_s} R_a$, with mean and variances

$$\begin{aligned}\mu_{\Re\{\hat{z}\}} = 1, \quad \sigma^2_{\Re\{\hat{z}\}} = \frac{\sum_{a\in\mathcal{A}_s} \alpha_a^{-2} \sigma^2_{\Re\{z_a\}}}{\left(\sum_{a\in\mathcal{A}_s} R_a\right)^2}, \\ \mu_{\Im\{\hat{z}\}} = 0, \quad \sigma^2_{\Im\{\hat{z}\}} = \frac{\sum_{a\in\mathcal{A}_s} \alpha_a^{-2} R_a(\sigma_a^4 + 2\alpha_{n,a}\sigma^2_{\nu,a})}{2\left(\sum_{a\in\mathcal{A}_s} R_a\right)^2}.\end{aligned} \tag{23}$$

F. Derivation of the SER, BER and SINR

Due to the symmetry of DMPSK constellations, the SER (P_s) and SINR (ρ) of the constellation can be calculated using any symbol of the constellation. In this case, we particularize for the symbol $s = 1$, as done in Section III-B, without loss of generality. The SER can be approximated by following the approach in Appendix A of [4] as

$$P_s(\mathcal{A}_s) \approx 1 - \frac{\int_{-\pi/M}^{\pi/M} \int_0^{\infty} e^{-\left(\frac{r\cos(\gamma)-\mu_{\Re}}{\sqrt{2}\sigma_{\Re}}\right)^2} e^{-\left(\frac{r\sin(\gamma)-\mu_{\Im}}{\sqrt{2}\sigma_{\Im}}\right)^2} r dr d\gamma}{2\pi\sigma_{\Re}^2\sigma_{\Im}^2}. \tag{24}$$

As shown in Appendix A, we can simplify the double integral of (24) into a one dimensional integral as

$$P_s(\mathcal{A}_s) \approx 1 - \int_{-\pi/M}^{\pi/M} e^{-c} \frac{\sqrt{\pi} b e^{\frac{b^2}{4a}} \left(\operatorname{erfc}\left(\frac{b}{2\sqrt{a}}\right) + 1\right) + 2\sqrt{a}}{8\pi\sigma_{\Re}^2\sigma_{\Im}^2 a^{3/2}} d\gamma. \tag{25}$$

where a, b and c are defined in Appendix A. The integral in eq. (25) can be solved numerically while a closed-form expression is mathematically intractable.

The effective SNR ρ can be calculated as the inverse of the sum of the variances of the real and imaginary parts of the received symbol z^n, as shown in (26). We can further approximate (25) to a closed-form expression that does not require a numerical evaluation by assuming a circularly symmetric complex Gaussian distribution whose variance is half of $\sigma_{\Re}^2+\sigma_{\Im}^2$, and using the expression for PSK error probability of [24] as

$$P_s(\mathcal{A}_s) \approx 2Q\left(\sqrt{2\rho}\sin\left(\frac{\pi}{M}\right)\right). \tag{28}$$

Last but not least, the BER can be straightforwardly calculated assuming Gray mapping as $P_b(\mathcal{A}_s) = P_s(\mathcal{A}_s)/\log_2(M)$.

G. Remarks about the effects of spatial correlation

Assuming $\alpha_a = 1$ for all APs, the results agree with those obtained in [12]. Furthermore, for $A = 1$ and uncorrelated Rayleigh fading $\left(\bar{\mathbf{h}}_a, \sigma_{h,a}^2\mathbf{R}_a\right) = (\mathbf{0}_a, \mathbf{I}_a)$, we obtain the results of Appendix A of [4]. Assuming a specific model, for which $\left[\mathbf{R}_a\right]_{r_a,r'_a} = \delta_a^{|r_a - r'_a|}$ with $0 \le \delta_a \le 1$, where $|r_a - r'_a|$ is the distance between the antennas r_a and r'_a in AP a, the terms $||\mathbf{R}_a||_2^2$ and $\mathbf{1}^T\mathbf{R}_a\mathbf{1}$ are simplified to

$$R_a(\delta_a = 0) \le ||\mathbf{R}_a||_2^2 = R_a\frac{1-\delta_a^{2R_a}}{1-\delta_a^2} \le R_a^2(\delta_a = 1), \tag{29}$$

$$R_a(\delta_a = 0) \le \mathbf{1}^T\mathbf{R}_a\mathbf{1} = R_a\frac{1-\delta_a^{R_a}}{1-\delta_a} \le R_a^2(\delta_a = 1). \tag{30}$$

Moreover, any spatial correlation effect (defined by the spatial correlation matrix $\mathbf{R}_a$) may be adjusted to the model $\left[\mathbf{R}_a\right]_{r_a,r'_a} = \delta_a^{|r_a - r'_a|}$ by selecting an appropriate value for δ_a, allowing to perform analysis by just considering such model. If correlation increases, both eqs. (29) and (30) increase, thus increasing $\sigma_{\Re\{z_a\}}^2$, which worsens the SER performance and decreases ρ. For the extreme cases of $\delta_a = 0$ and $\delta_a = 1$, the SNR ρ is shown in eq. (27). For $\delta_a = 1$, each AP has just one effective antenna regarding spatial correlation effects, so the ρ will grow more slowly since only the noise will linearly decrease. Contrarily, for $\delta_a = 0$, which is shown in the left-hand side of eq. (27), the performance tends to improve linearly with the total number of antennas of all APs. Besides, it can be observed in both cases that the last term of the denominator tends to 0 by increasing K_a ($|\bar{h}_a|^2$ tends to 1 and $\sigma_{h,a}^2$ to 0), so a strong Rician component enhances the performance. Interestingly, these conclusions are similar to those obtained for coherent CF schemes in [25]. Last but not least, Eq. (27) for $\sigma_{\nu,a}^2 = 0$ (no noise) and a Rayleigh channel ($\sigma_{h,a}^2 = 1$ and $|\bar{h}_a|^2$) results in $\rho = \left(\sum_{a\in\mathcal{A}_s} R_a\right)^2 / \left(\sum_{a\in\mathcal{A}_s} R_a^2\right)$. Therefore, in the right-hand side of (27) for the worst case of $\delta_a = 1$, the numerator tends to grow with the square of the sum of the number of antennas in each AP while the denominator with the sum of the square of the number of antennas in each AP. Nonetheless, the square of a sum always grows faster than the sum of squares, so the performance tends to improve when several spatially uncorrelated APs are used, for the same number of total antennas.

Even though utilizing several uncorrelated APs will potentially benefit the NC scheme, this will not always be true if we consider a limited total number of antennas, since the number of APs will be finite with each AP having a finite number of antennas and a different path loss (larger attenuation will result in lower SNR, for the same number of antennas). Therefore, it will be necessary to analyze each scenario to validate whether processing with all the APs is better than with a subset of the APs.

IV. Cell-free AP selection in Non-coherent Massive SIMO based on DMPSK

In this section, we propose four alternatives to select a subset $\mathcal{A}_s$ among a set of accessible APs $\mathcal{A}$ to maximize the performance of the coordinated multipoint reception in NC-mSIMO. The first one is a brute force search (BFS) which tests all the possible AP combinations, so it is the best in terms of performance but the most complex one. The second one performs a successive AP selection (SAPS) in a greedy way, so it has a lower performance and a lower complexity than the BFS. The last one performs a simplified successive AP selection (each iteration tests including the next best AP), so it is the one with the worst performance but also the one with the lowest complexity. A fourth proposed alternative, even though not explained, is to select all the "visible" APs by the user. We will show the performance and complexity via simulations in Section VI.

The z_a of $\mathcal{A}_s$ are sent to the CPU and processed following (6). The performance measure in our case will be P_s, defined in (25). The goal is to select a subset $\mathcal{A}_s$ among a set of accessible APs $\mathcal{A}$ so that (25) is minimized. We define the following optimization problem, which is discrete and deterministic

$$\begin{aligned} \min_{\mathcal{A}_s, \Upsilon_{\mathcal{A}_s}} \quad & f_{\text{obj}} = P_s(\mathcal{A}_s), \\ \text{s.t.} \quad & \mathcal{A}_s \in \mathcal{A}, \quad |\mathcal{A}_s| = A_s, \\ & \Upsilon_{\mathcal{A}_s} = \{K_{\mathcal{A}_s}, \alpha_{\mathcal{A}_s}, \sigma_{\nu,\mathcal{A}_s}, R_{\mathcal{A}_s}, \mathbf{R}_{\mathcal{A}_s}\}, \end{aligned} \tag{31}$$

$$\rho = \frac{\left(\sum_{a\in\mathcal{A}_s} R_a\right)^2}{\sum_{a\in\mathcal{A}_s}\left(R_a(\sigma^4_{\nu,a}+2\alpha_a\sigma^2_{\nu,a})+\alpha_a^2\sigma^2_{h,a}(\sigma^2_{h,a}\,||\mathbf{R}_a||_2^2+2|\bar{h}_a|^2\mathbf{1}^T\mathbf{R}_a\mathbf{1})\right)} \tag{26}$$

$$\underset{\delta_a=0}{\rho} = \frac{\left(\sum_{a\in\mathcal{A}_s} R_a\right)^2}{\sum_{a\in\mathcal{A}_s} R_a\left(\sigma^4_{\nu,a}+2\alpha_a\sigma^2_{\nu,a}+\alpha_a^2\sigma^2_{h,a}(1+|\bar{h}_a|^2)\right)} \quad \underset{\delta_a=1}{\rho} = \frac{\left(\sum_{a\in\mathcal{A}_s} R_a\right)^2}{\sum_{a\in\mathcal{A}_s} R_a\left(\sigma^4_{\nu,a}+2\alpha_a\sigma^2_{\nu,a}+R_a\alpha_a^2\sigma^2_{h,a}(1+|\bar{h}_a|^2)\right)} \tag{27}$$

TABLE I
COMPLEXITY OF DIFFERENT APS SELECTION TECHNIQUES

Technique	Compl.	A=1	A=5	A=10	A=20	A=300
BFS max	2^A-1	0	31	1023	1M	$2^{300}\approx\infty$
SAPS max	$\frac{A^2+A}{2}$	0	15	55	210	45K
SAPS min	$2A-1$	0	9	19	39	599
sSAPS max	$2A-1$	0	9	19	39	599
sSAPS min	$A+1$	0	6	11	21	301

where A_s is the cardinality of subset $\mathcal{A}_s$ and $\Upsilon_{\mathcal{A}_s}$ is a set of parameters of the subset $\mathcal{A}_s$, needed by the CPU to select the best subset. These parameters are, for each AP in $\mathcal{A}_s$, the Rician factors $K_{\mathcal{A}_s}$, the square of the large-scale fading $\alpha_{\mathcal{A}_s}$, the noise power $\sigma_{\nu,\mathcal{A}_s}$, the number of antennas $R_{\mathcal{A}_s}$ and the channel spatial correlation matrix $\mathbf{R}_{\mathcal{A}_s}$. The channel parameters required to solve the optimization problem defined in (31) vary in a very large temporal scale. The subsets $\mathcal{A}_s$ can have 1 to A APs, with a total combinations of 2^A-1 possible different subsets.

The computation of P_s depends on M, which is the constellation size of DMPSK. For fixed $\sigma^2_{\Re}$ and $\sigma^2_{\Im}$, a larger M results in a smaller integration area so a larger P_s, and viceversa. Therefore, we just have to compute the P_s for one constellation size and the effects of $\sigma^2_{\Re}$ and $\sigma^2_{\Im}$ will be the same for other constellation sizes.

A. Brute-force search (BFS) AP Selection

The optimization problem defined in (31) may be solved via a brute force search to obtain the set $\mathcal{A}_s^{\min}$, which is the APs set that minimizes the symbol error probability. This approach gives the best performance in terms of BER, while its main limitation is its complexity. It needs to calculate P_s in (25) a total of $\sum_{a=1}^{A}\frac{A!}{a!(A-a)!}=2^A-1$ times. This is caused by the fact that we must look for combinations without repetitions of A APs. Nevertheless, this solution is useful since it represents an upper-bound in terms of performance, useful to compare it with suboptimal solutions. A pseudocode for the brute force search is provided in Algorithm 1.

Algorithm 1 Brute Force Search APs Selection

procedure selectAP$_\mathbf{B}$FS($\mathcal{A}_s$, $\Upsilon_{\mathcal{A}_s}$)
  $[\hat{\mathcal{A}}_\mathbf{s}] \leftarrow$ createAllCombs($\mathcal{A}_s$) ▷ *Create All Combinations*
  $[\boldsymbol{P}_{\boldsymbol{s},\hat{\mathcal{A}}_\mathbf{s}}] \leftarrow$ computePs($\hat{\mathcal{A}}_\mathbf{s}$, $\Upsilon_{\mathcal{A}_s}$) ▷ *Compute P_s of $\hat{\mathcal{A}}_\mathbf{s}$*
  $[\hat{\mathcal{A}}_\mathbf{s}^{\min}] \leftarrow$ selectMinPs($\boldsymbol{P}_{\boldsymbol{s},\hat{\mathcal{A}}_\mathbf{s}}$,$\hat{\mathcal{A}}_\mathbf{s}$) ▷ *Select AP set with minimum P_s*
  return $[\hat{\mathcal{A}}_\mathbf{s}^{\min}]$ ▷ *Return base station set with minimum P_s*
end procedure

B. Successive AP selection (SAPS)

One possibility to obtain a good performance while keeping the complexity low is to perform a greedy algorithm that successively selects the APs in the following way (see Algorithm 2). Please note greedy algorithms [26], which obtain a global optimal solution by doing several subsequent local optimal choices, have been applied in other selection strategies problems, such as hybrid precoding [27] to select the optimal beamforming vectors of a codebook by avoiding an exhaustive search. By contrast, in this section, we adapt the greedy algorithm to use it to search for an optimal set of serving APs for the non-coherent cell-free approach. First, the AP with the lowest individual P_s (called $P_{s,1}$) is selected, and is named A_1. A total of A calculations of P_s are needed in this first iteration. Among the $A-1$ APs left, we select the one that, combined with A_1, further reduces the P_s (called $P_{s,2}$), needing a total of $A-1$ calculations. This process is repeated until $P_{s,i} > P_{s,i-1}$ or until all APs are included in the set. The maximum complexity of this approach would be $\sum_{i=0}^{A-1}(A-i)=\frac{A^2+A}{2}$ computations, while the minimum complexity would be $2A-1$, which is the case in which not a single second AP improves the performance.

Algorithm 2 Successive AP selection (SAPS)

procedure selectAP$_\mathbf{S}$APS($\mathcal{A}_s$, $\Upsilon_{\mathcal{A}_s}$)
  $[\boldsymbol{P}_\boldsymbol{s}] \leftarrow$ computePs($\mathcal{A}_\mathbf{s}$, $\Upsilon_{\mathcal{A}_s}$) ▷ *Compute P_s of $\mathcal{A}_\mathbf{s}$*
  $[\tilde{\boldsymbol{P}}_\boldsymbol{s},\tilde{\mathcal{A}}_\mathbf{s},\tilde{\Upsilon}_{\mathcal{A}_s}] \leftarrow$ orderPsAs($\boldsymbol{P}_\boldsymbol{s}$,$\mathcal{A}_\mathbf{s}$,$\Upsilon_{\mathcal{A}_s}$) ▷ *Order APs*
  $[\boldsymbol{P}^{\min}_{\boldsymbol{s},0}, \boldsymbol{P}^{\min}_{\boldsymbol{s},1}] \leftarrow [1, \tilde{\boldsymbol{P}}_\boldsymbol{s}(1)]$ ▷ *Init Ps min to 1 and 1^{st} Ps*
  i $\leftarrow$ 1, set $\leftarrow$ 1 ▷ *Initialize Iter*
  while $\boldsymbol{P}^{\min}_{\boldsymbol{s},i} < \boldsymbol{P}^{\min}_{\boldsymbol{s},i-1}$ **do** ▷ *Loop over all APs*
    i $\leftarrow$ i + 1
    for k from (i to A) - set **do** ▷ *Loop in each iteration*
      [setTemp2,setTemp] $\leftarrow$ [set,[set,k]]
      $[\boldsymbol{P}^{\text{temp}}_{\boldsymbol{s}}] \leftarrow$ computePs($\tilde{\mathcal{A}}_\mathbf{s}$(setTemp),$\tilde{\Upsilon}_{\mathcal{A}_s}$(setTemp))
      if $\boldsymbol{P}^{\text{temp}}_{\boldsymbol{s}} < \boldsymbol{P}^{\min}_{\boldsymbol{s},i}$ **then**
        $\boldsymbol{P}^{\min}_{\boldsymbol{s},i} \leftarrow \boldsymbol{P}^{\text{temp}}_{\boldsymbol{s}}$
        setTemp2 $\leftarrow$ setTemp
      end if
    end for
    set $\leftarrow$ setTemp2 ▷ *Update set of APs with min Ps*
    $\tilde{\mathcal{A}}^{\min}_\mathbf{s} \leftarrow \tilde{\mathcal{A}}_\mathbf{s}$(set) ▷ *Assign set of min Ps*
  end while
  return $[\tilde{\mathcal{A}}^{\min}_\mathbf{s}]$ ▷ *Return base station set with minimum P_s*
end procedure

C. Smart Successive AP selection (sSAPS)

The last proposal to obtain a good performance while keeping the complexity low is to perform a successive selection of APs in a smart way (see Algorithm 3). This method can

be seen as a simplified greedy approach in which the APs are successively selected taking into account their individual performance, from better to worse. The P_s of all APs is computed and they are sorted in ascending order, taking a total of A computations of P_s. The AP with the lowest individual P_s (called $P_{s,1}$) is selected and is named A_1. The AP with the second lowest P_s is combined with A_1 and the P_s of the combination is calculated and named $P_{s,2}$. This process is repeated until $P_{s,i} > P_{s,i-1}$ or until all APs are included in the set. The maximum complexity of this approach would be $2A-1$, which results from computing the P_s until all APs are included in the set. The minimum complexity would be $A+1$, when the second AP does not reduce the overall P_s.

Algorithm 3 Smart Successive AP selection (sSAPS)

procedure selectAPsBFS($\mathcal{A}_s$, $\Upsilon_{\mathcal{A}_s}$)
  $[\boldsymbol{P_s}] \leftarrow$ computePs($\mathcal{A}_\mathbf{s}$, $\Upsilon_{\mathcal{A}_s}$) ▷ *Compute P_s of $\mathcal{A}_\mathbf{s}$*
  $[\tilde{\boldsymbol{P}}_\boldsymbol{s}, \tilde{\mathcal{A}}_\mathbf{s}, \tilde{\Upsilon}_{\mathcal{A}_s}] \leftarrow$ orderPsAs($\boldsymbol{P_s}$,$\mathcal{A}_\mathbf{s}$,$\Upsilon_{\mathcal{A}_s}$) ▷ *Order APs*
  $[\boldsymbol{P}^{\min}_{\boldsymbol{s},0}, \boldsymbol{P}^{\min}_{\boldsymbol{s},1}] \leftarrow [1, \tilde{\boldsymbol{P}}_\boldsymbol{s}(1)]$ ▷ *Init Ps min to 1 and 1^{st} Ps*
  i $\leftarrow$ 1 ▷ *Initialize Iter*
  while $\boldsymbol{P}^{\min}_{\boldsymbol{s},i} < \boldsymbol{P}^{\min}_{\boldsymbol{s},i-1}$ **do** ▷ *Loop*
    $[\boldsymbol{P}^{\min}_{\boldsymbol{s}}, \tilde{\mathcal{A}}^{\min}_{\mathbf{s}}] \leftarrow [\boldsymbol{P}^{\min}_{\boldsymbol{s},i}, \tilde{\mathcal{A}}_\mathbf{s}(1{:}i)]$ ▷ *Assign min Ps*
    i $\leftarrow$ i + 1
    $[\boldsymbol{P}^{\min}_{\boldsymbol{s},i}] \leftarrow$ computePs($\tilde{\mathcal{A}}_\mathbf{s}(1{:}i)$,$\tilde{\Upsilon}_{\mathcal{A}_s}(1{:}i)$) ▷ *$1^{st}$ to i^{th} Ps*
  end while
  return $[\tilde{\mathcal{A}}^{\min}_{\mathbf{s}}]$ ▷ *Return base station set with minimum P_s*
end procedure

D. Figure of Merit (FoM) to compare selection techniques

We first compare the APs selection methods in terms of complexity resulting in sSAPSmin < sSAPSmax = SAPSmin < SAPSmax < BFS, so

$$A+1 \leq 2A-1 \leq \frac{(A+1)A}{2} \leq 2^A - 1 \rightarrow A \geq 2. \tag{32}$$

Then, to compare the techniques accounting for both the complexity (C), either time or computational, and the performance of each technique, we formulate

$$FoM = \left(-\log_{10}(P_s)\right)^{-1} \times 100C, \tag{33}$$

which serves as a figure-of-merit (FoM) decision variable between techniques. A multiplication by 100 is done to avoid rounding errors in the results. Lower P_s come at the expense of greater complexity, but it may be possible that the P_s does not increase much while complexity greatly reduces. This FoM is useful in fast varying channels in which we aim at minimizing the AP selection execution time in the CPU.

V. Parameters for Performance Comparison between Non-coherent CF and Coherent CF

The aim of this section is to show that, in deployment scenarios of stringent conditions, such as fast varying channels and/or low SNR, the NC-CF proposal can outperform its coherent counterpart. First, we explain the baseline coherent CF mSIMO with a minimum mean square error (MMSE)-based fully centralized processing scheme. Then, we consider the channel estimation overhead problem of any coherent CF scheme. Later, we do a qualitative analysis of the delay and complexity. Last, we describe the performances of the coherent and NC schemes in terms of BER.

A. Baseline coherent cell-free massive SIMO

We consider the optimal approach in terms of ρ for the coherent CF scheme, which is the MMSE-based fully centralized processing scheme (see [28] and references therein). It requires tight synchronization between APs, large computational resources, and fronthaul links capable of managing a considerable amount of data traffic. Notice there are plenty of other processing strategies when it comes to coherent CF, such as the commonly used distributed maximum ratio (MR) processing [18], but, in order to maintain fairness in comparison, we are only showing the MMSE-based as it represents the spectral efficiency upper-bound.

In contrast to NC-CF-mSIMO, its coherent counterpart requires performing channel estimation (which can be either performed locally at each AP or at the CPU) for the later construction of the combining vector. During the UL training phase, the user terminal will send its pilot signal to every AP resulting in

$$\mathbf{y}^n_{p,a} = \mathbf{h}^n_a \boldsymbol{\varphi}^n + \boldsymbol{\nu}^n_{p,a}, \tag{34}$$

as the received training signal at AP a during time instant n. The unique pilot sequence is $\boldsymbol{\varphi}^n \in \tau_p \times 1$, while τ_p are the pilot resources allocated for the channel estimation and $\boldsymbol{\nu}^n_{p,a}$ is the additive white gaussian noise (AWGN) term at time instant n whose entries are distributed as $\mathcal{CN}(0, (\sigma^n_{p,a})^2)$. In the centralized MMSE scheme, each AP will typically act as a relay that forwards $\mathbf{y}^n_{p,a}$ to the CPU for channel estimation. The channel estimates will be acquired by MMSE estimation [29] and will be distributed as $\mathbf{h}^n_a \sim \mathcal{CN}(\bar{\mathbf{h}}^n_a, \tau_p(\sigma^n_{p,a})^{-2}\mathbf{R}^n_a(\boldsymbol{\Psi}^n_a)^{-1}\mathbf{R}^n_a)$. The channel estimation error is $\mathbf{e}^n_a = \boldsymbol{h}^n_a - \hat{\mathbf{h}}^n_a$ which follows $\mathbf{e}^n_a \sim \mathcal{CN}(\mathbf{0}_{R_a}, \mathbf{E}^n_a)$ with $\mathbf{E}^n_a = \mathbf{R}^n_a - \tau_p(\sigma^n_{p,a})^{-2}\mathbf{R}^n_a(\boldsymbol{\Psi}^n_a)^{-1}\mathbf{R}^n_a$. Thanks to the MMSE channel estimate we ensure that $\mathbf{e}^n_a$ and $\hat{\mathbf{h}}^n_a$ are independent, the same as $\mathbf{h}^n_a$ and $\hat{\mathbf{h}}^n_a$ (a necessary condition for the definition of ρ_c that will be shown in (38)). The channel estimate is then

$$\begin{aligned}\hat{\mathbf{h}}^n_a &= \bar{\mathbf{h}}^n_a + \frac{\mathbb{E}\left\{\check{\mathbf{y}}^n_{p,a}(\check{\mathbf{h}}^n_a)^H\right\}}{\mathbb{E}\left\{\check{\mathbf{y}}^n_{p,a}(\check{\mathbf{y}}^n_{p,a})^H\right\}}\check{\mathbf{y}}^n_{p,a} \\ &= \bar{\mathbf{h}}^n_a + \sqrt{\tau_p(\sigma^n_{p,a})^{-2}}\mathbf{R}^n_a(\boldsymbol{\Psi}^n_a)^{-1}\check{\mathbf{y}}^n_{p,a},\end{aligned} \tag{35}$$

with $\check{\mathbf{h}}^n_a = \mathbf{h}^n_a - \mathbb{E}\left\{\mathbf{h}^n_a\right\}$, and $\boldsymbol{\Psi}^n_a \triangleq (\sigma^n_{p,a})^{-2}\mathbf{R}^n_a + \mathbf{I}_{R_a}$.

During the UL data payload phase, the user will send its data symbol to every AP and each AP to the CPU, i.e.

$$\mathbf{y}^n_a = \mathbf{h}^n_a x^n + \boldsymbol{\nu}^n_a, \tag{36}$$

where $\boldsymbol{\nu}^n_a$ accounts for the AWGN term during time instant n and is distributed as $\mathcal{CN}\left(0, (\sigma^n_a)^2\right)$. We can express the decoded data symbol during the UL data payload phase as

$$\hat{x}^n = \sum_{a=1}^{A}\left(\mathbf{b}^n_a\right)^H \mathbf{y}^n_a = \sqrt{\rho_u}\sum_{a=1}^{A}\left(\mathbf{b}^n_a\right)^H \mathbf{h}^n_a x^n + \left(\mathbf{b}^n_a\right)^H \mathbf{r}^n_a, \tag{37}$$

where the combining vector $\mathbf{b}_a^n$ must be searched to maximize the ρ of $\hat{x}^n$. Given the instant CSI knowledge at the CPU and defining $\mathbf{E}^n = \text{diag}(\mathbf{E}_1^n, \ldots, \mathbf{E}_A^n)$ and using [3] we have

$$\rho_c = \frac{(\sigma_{u,a}^n)^{-2} \left|(\mathbf{b}_a^n)^H \hat{\mathbf{h}}_a^n\right|^2}{(\mathbf{b}_a^n)^H \left((\sigma_{p,a}^n)^{-2}\mathbf{E}^n + \mathbf{I}_{AR_a}\right) \mathbf{b}_a^n}. \tag{38}$$

Defining $\mathbf{h}^n = \left[\mathbf{h}_1^n, \ldots, \mathbf{h}_A^n\right]$, and as shown in [3], the combining vector that maximizes (38) is

$$\begin{aligned}\mathbf{b}^n &= \left[\mathbf{b}_1^n, \ldots, \mathbf{b}_A^n\right] \\ &= (\sigma_{p,a}^n)^{-2} \left((\sigma_{p,a}^n)^{-2} \left(\hat{\mathbf{h}}^n (\hat{\mathbf{h}}^n)^H + \mathbf{E}^n\right) + \mathbf{I}_{AR_a}\right)^{-1} \hat{\mathbf{h}}^n.\end{aligned} \tag{39}$$

B. Channel estimation overhead

Assuming a total of τ_c wireless resources in a coherence block and τ_p pilot resources needed for the channel estimation, the efficiency of the link, caused by the pilot usage is

$$\tau = 1 - \frac{\tau_p}{\tau_c}. \tag{40}$$

If τ_c is close to τ_p, the efficiency of a coherent approach will be very low, even zero in the extreme case ($\tau_p = \tau_c$), as shown in [4]. Contrarily, $\tau_p = 0$ is always true for the NC scheme since it will not have any pilot overhead.

C. Delay and complexity of the detection

Not only does the channel estimation reduce the efficiency of the link, but it also increases the delay in the data reception with the channel estimation delay t_{chEst}. Once the channel is estimated, it must be compensated with any of the filtering/precoding techniques in the literature, taking a compensation time t_{comp}. Then, there is a total delay of $t_{\text{chEst}} + t_{\text{comp}}$ before the data can be detected. On the contrary, the NC scheme only needs to perform the differential decoding and averaging, which is lower than t_{comp}, as shown in [13].

Yet another aspect of controversy of coherent CF schemes is their computational demands together with the usage of the fronthaul links. Each AP is required to send $\tau_p R_a$ complex scalars to the CPU for channel estimation, while the CPU itself will be required to perform $(R_a + R_a^2)A$ complex multiplications for computing channel estimates. On the other side, APs will send $(\tau_c - \tau_p)R_a$ complex scalars to the CPU for the UL data reception. Last but surely not least, the computation complexity of the MMSE combining vector will grow cubically with R_a and A. Please, refer to [30], among other references, for a better understanding of the computational needs in coherent CF mSIMO networks. Comparatively, the complexity of the NC-CF scheme is much lower. Each AP will perform R_a complex multiplications and a complex summation of R_a terms. It will send one complex scalar (z_a) to the CPU, which will only perform the summation of a maximum of A complex values. It is clear that the computational complexity and the fronthaul overload are much lower for the NC than for the coherent counterpart.

D. Performance comparison

A higher complexity of the coherent processing is justified when the performance is clearly improved. However, we will show that there are situations when this is not the case. Thus, to compare the coherent and NC-CF schemes in terms of performance, we will use the SER. Our intention is to use a realistic measure to compare among schemes. In order to make fair comparisons, the same data efficiency must be ensured for both the coherent and the NC schemes. This same data efficiency can be obtained by adjusting the effective ρ according to the channel estimation overhead. The SER of the NC is defined using (25), and the SER of the coherent scheme will be defined following [24] as

$$P_{s,c} = 2Q\left(\sqrt{2\tau\rho_c}\sin\left(\frac{\pi}{M_c}\right)\right), \tag{41}$$

where ρ_c denotes the SINR of the coherent scheme after joint processing and is calculated as (38). The τ factor is included to adjust its value accounting for some resources that are used for channel estimation. Let us clarify this with an example: assume the number of symbols available for the UL of a TDD system, due to the coherence time length, is 2 symbols. In this case, for the coherent scheme at least one symbol is needed for channel estimation while the other one is needed for data transmission, while for the NC scheme, both symbols could be used for data. Thus, to obtain the same data efficiency, the overhead parameter would be set to $\tau = 0.5$ to adjust the effective ρ_c to compute the $P_{s,c}$.

Even though it is out of the scope of this work, another problem with the coherent scheme is the channel estimation error, which comes from the fact that the estimated channel is imperfect, caused by several reasons, including but not limited to noisy estimation and channel variability [31].

VI. Numerical Results

In this section, we show numerical results. First, we verify our analysis of the symbol error probability P_s and the SINR ρ. Second, we show a comparison in terms of performance and complexity for the different APs selection techniques developed in Section IV, and show that the computation time relates directly to the complexity. Last, we show the performance in a scenario with realistic 3D MIMO channels and a realistic AP deployment, to show that our proposal can outperform the coherent CF massive MIMO scheme in fast varying channels and/or low SNRs.

The results in this section are obtained for a constellation size $M = 4$, a maximum of 8 available APs and a random number of antennas in each AP between 1 and 256 (in powers of 2), selected randomly. The user is placed at the centre of a 100m x 100m square, and the APs are uniformly placed in this square at each iteration of the Monte Carlo simulation. The path loss follows a simplified version of the 3GPP urban microcell described in [32]. It is expressed as $L_a^n = L_0 + 10p\log_{10}(d_a^n) + \chi_a^n$, where L_0 is the path loss at a reference distance of 1 meter, p is the path loss exponent that depends on the environment, d_a^n is the distance between the centre of the array of the AP a and the user and χ_a^n is the shadow

fading component which is modelled as $\chi_a^n \sim \mathcal{N}(0, \sigma^2_{\chi_a^n})$. Thus, the channel gain is defined as $\alpha_a^n = 10^{-L_a^n/10}$. The Rician factor K_a^n is distributed as $10\log_{10}(\mathcal{K}_a^n) \sim \mathcal{N}\left(\mu_{\mathcal{K}_a^n}, \sigma^2_{\mathcal{K}_a^n}\right)$. The spatial correlation of the NLoS component is defined by δ_a^n and follows a random uniform distribution between 0 and 1 for each AP. All these parameters are used as described in the following sections unless otherwise stated.

A. Corroboration of Statistical Analysis for BER and SINR

In this section, we check that the theoretical analysis of the BER and SINR is correct and we get some insights on the effect of spatial correlation on the performance of NC-mSIMO when a multi-AP processing is performed. We show both the theoretical and the Monte-Carlo (obtained via simulations) results of the BER and SINR for the correlation model defined in Section III-G. Some channel parameters are fixed and modified with respect to the previous description, for representation purposes.

First and foremost, we have performed a Kolmogorov-Smirnov (KS) test to check if both the theoretical and the Monte-Carlo distributions obtained for z are the same. When $\delta_a < 0.93$, values that can be regarded as representatives of realistic channels, the theoretical and Monte-Carlo distributions were almost the same for a standard significance value of 5%, confirming our analysis. On the contrary, for $\delta_a > 0.93$, the test for the real part of the distribution fails, which indicates that the distributions cannot be regarded as the same. Nevertheless, the goal is to check whether the analysis is valid for the BER and the SINR and to check if there is a discrepancy between the theoretical and Monte Carlo results. Figs. 1 and 2 show that even though the discrepancy between the BER and SINR obtained by simulations and with the analysis in Section III is greater for high values of δ_a, the approximations still provide accurate results. The small discrepancy comes from the fact that the approximation of Gamma to Gaussian distributions is less valid with larger spatial correlations.

Fig. 1 shows the BER for $K_a = 2$, against δ from 0.7 to 1, for $\bar{\rho} = -5$ dB and $\bar{\rho} = 10$ dB, with and without path loss compensation. Interestingly, the path loss compensation works better in higher $\bar{\rho}$ values. The reason for this is the noise enhancement that results from path loss compensation when the noise is high. Both simulations and theoretical values are shown. We can observe how the BER increases with δ_a, since channel hardening is reduced. In Fig. 2, we can observe the $\bar{\rho}$ from the theoretical analysis and the Monte Carlo simulation versus different ρ_a (the same for all APs), for $K_a = 2$ for all APs, with and without path loss compensation. The same conclusions can be extracted as those for Fig. 1. A very good agreement can be found in both figures for the theoretical analysis and the Monte Carlo simulation.

B. AP selection in NC-CF for 8 APs

This section shows how the different proposed AP selection techniques behave. The noise power $(\sigma_a^n)^2$ is defined such that the mean SNR in the APs goes from -10 dB to 35 dB.

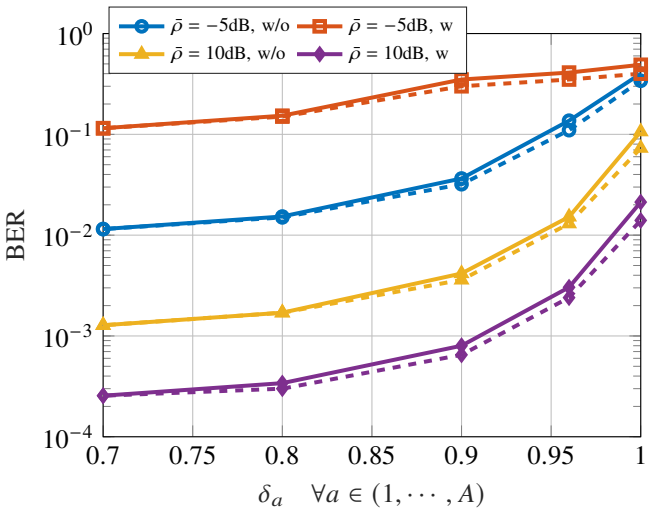

Fig. 1. BER vs δ_a for $K_a = 2$ $\forall a \in (1, \cdots, A)$ and two different effective SNR $\bar{\rho}$ values, with (w) and without (w/o) pathloss compensation. Monte Carlo (dashed line) versus theoretical analysis (continuous line).

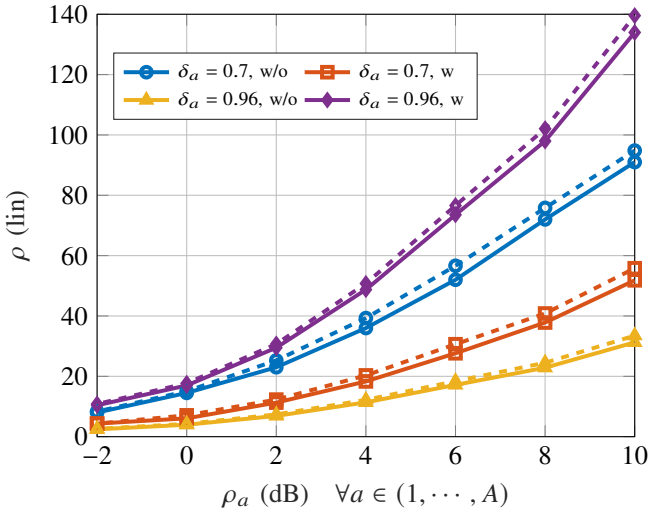

Fig. 2. ρ (linear) vs ρ_a for $K_a = 2$ $\forall a \in (1, \cdots, A)$ and two different δ_a values, with (w) and without (w/o) pathloss compensation. Monte Carlo (dashed line) versus theoretical analysis (continuous line).

TABLE II
BER, TIME, NOPS AND FOM FOR DIFFERENT AP SELECTION TECHNIQUES FOR A=8 AND $\bar{\rho}$ = 10 DB WITH PATH LOSS COMPENSATION.

Technique	BER ($\bar{\rho}$ = 10dB)	Time (secs)	Nops	FoM
One AP	7.53e-03	0.24	8	12
All AP	2.03e-04	0.07	1	2
BFS	1.14e-06	13.5	255	227
SAPS	8.1e-06	2.53	15-36	50
sSAPS	2.12e-05	0.42	9-15	9

We show how the BFS approach outperforms the SAPS and the SAPS outperforms the sSAPS in terms of BER performance, while the opposite happens for the complexity. By looking at Table II, one can see how the technique that takes the longest is the BFS, followed by the SAPS and ending with the sSAPS which is the one that takes the least time. Comparatively, the All AP approach is better than the single AP but worse than the others, which remarks the fact that

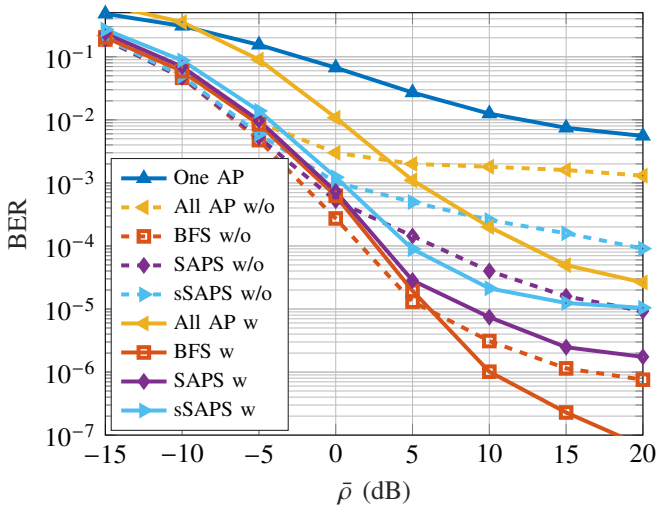

Fig. 3. BER vs mean SNR in dB for 8 APs comparing with (continuous line) and without (dashed line) path loss compensation in each AP.

some APs will potentially decrease the overall performance, mainly because they are at a very large distance, do not have enough antennas to compensate the large path loss and/or high noise or have a very high spatial correlation. That is why an AP selection technique is of interest. Consequently, the performance is best for the BFS, followed by the SAPS and ending with the sSAPS, which has the lowest performance. This fact is supported by looking at Fig. 3, which shows the performance when path loss compensation is and is not performed locally at each AP before combination processing at the CPU. The path loss compensation in each AP before the central combination processing affects the performance, is better not to compensate the path loss in the low SNR, while in the medium to large SNR it is convenient to compensate. To summarize, the best BER is given by the BFS, then the SAPS, then the sSAPS and last the All AP.

Nevertheless, to make a fair comparison among techniques, we utilize the FoM defined in Section IV-D, for which the lower the value, the better the technique. By looking again at Table II, in which C from (33) has been substituted by the execution time, it can be seen how the best approach according to the FoM is the All AP followed by the sSAPS. Comparatively, the sSAPS increases the performance by about two orders of magnitude while less than doubling the execution time, with respect to the "One AP" approach. On the contrary, the decrement in performance with respect to the BFS is about two orders of magnitude but the execution time is about 28 times larger. While we do not include the results for a low $\bar{\rho}$ for space economy, the best approach will be the sSAPS.

C. AP selection in NC-CF for 1 to 7 APs

In this section, an increasing number of APs from 1 to 7 has been simulated to find out which AP selection approach is best in this range. We do not include graphical results for space economy. By looking at Table III, we can see how the BER performance is the best for the BFS, followed by the SAPS, then the sSAPS and finally de All AP. Contrarily, the execution time follows the opposite behaviour. Nevertheless, the FoM shows that the best approach that balances the execution time and the BER performance is the "All AP" selection technique. Similar to the previous section, for a low $\bar{\rho}$ the best approach will be the sSAPS.

TABLE III
COMPARISON OF DIFFERENT AP SELECTION TECHNIQUES FOR 2 TO 7 APS AND $\bar{\rho}$ = 10 DB WITH PATHLOSS COMPENSATION.

A	Technique	BER ($\bar{\rho}$ = 10dB)	Time (secs)	Nops	FoM
2	**One AP**	9,529e-02	0,057	2	5,6
	All AP	4,907e-03	0,046	1	2,0
	BFS	4,500e-03	0,182	3	7,7
	SAPS	4,903e-03	0,104	3	4,5
	sSAPS	4,903e-03	0,103	3	4,5
3	**One AP**	5,171e-02	0,086	3	6,7
	All AP	1,093e-03	0,051	1	1,7
	BFS	6,805e-04	0,392	7	12,4
	SAPS	8,637e-04	0,240	5-6	7,8
	sSAPS	1,009e-03	0,188	4-5	6,3
4	**One AP**	3,094e-02	0,113	4	7,5
	All AP	3,827e-04	0,055	1	1,6
	BFS	9,904e-05	0,797	15	19,9
	SAPS	1,608e-04	0,460	7-10	12,1
	sSAPS	2,653e-04	0,252	5-7	7,1
5	**One AP**	1,923e-02	0,143	5	8,3
	All AP	1,597e-04	0,057	1	1,5
	BFS	1,350e-05	1,623	31	33,3
	SAPS	3,456e-05	0,794	9-15	17,8
	sSAPS	9,327e-05	0,302	6-9	7,5
6	**One AP**	1,272e-02	0,164	6	8,6
	All AP	1,888e-04	0,058	1	1,5
	BFS	2,337e-06	3,208	63	57,0
	SAPS	1,340e-05	1,198	11-21	24,6
	sSAPS	7,527e-05	0,332	7-11	8,1
7	**One AP**	8,188e-03	0,198	7	9,5
	All AP	1,978e-05	0,061	1	1,3
	BFS	7,230e-07	6,780	127	110,4
	SAPS	8,436e-06	1,822	13-28	35,9
	sSAPS	1,533e-05	0,374	8-13	7,8

For fast varying channels, the best is to select the sSAPS for low $\bar{\rho}$ values and the "All AP" for high $\bar{\rho}$, the former without channel compensation and the latter with channel compensation. For slowly varying channels with low $\bar{\rho}$ the best is to avoid channel compensation and use the BFS or the SAPS for 2 to 4 APs since they have the best performance with a similar execution time. For 5 and 6 the best is to use the SAPS, for 7 and up to 20, the sSAPS is the best option. Last, for more than 20 APs the best is to utilize the "All AP" selection technique.

D. AP selection in NC-CF for 200 APs with $R_a = 1$

In this section, we simulate 200 APs with a single antenna, and perform all the proposed AP selection techniques except for the BFS, since the complexity is extremely large even for offline simulations.

By looking at Fig. 4, we can see that the best performance in the low $\bar{\rho}$ is obtained for the All AP, SAPS and sSAPS without path loss compensation or for the sSAPS and SAPS with path loss compensation. Please note the results for SAPS are included for illustration purposes since the complexity would still be very large. In the high $\bar{\rho}$ all the techniques with path loss compensation outperform the ones without it, and out of them, the All AP seems to be the best selection due to

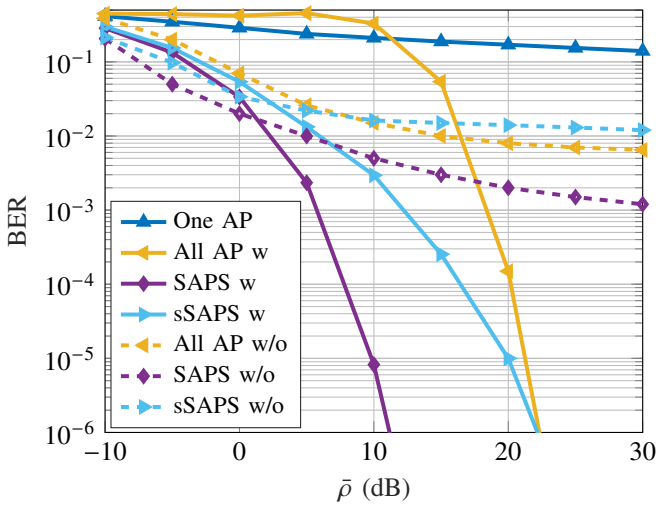

Fig. 4. BER vs mean SNR in dB for 200 single-antenna APs comparing with (continuous line) and without (dashed line) path loss compensation in each AP (no BFS shown due to complexity limitations).

TABLE IV
T_c TO T_s RATIO (N_{CT}), FOR v = 500 KM/H FOR DIFFERENT f_c IN GHZ AND Δ_f IN KHZ.

N_{CT}	Δ_f= 15	Δ_f= 30	Δ_f= 60	Δ_f= 120	Δ_f= 240
f_c = 0.7	7	15	29	-	-
f_c = 3.6	1.4	2.8	5.6	-	-
f_c = 27	-	-	-	1.5	3

the fact that it has no complexity in terms of AP selection but performs very well. In the intermediate $\bar{\rho}$ range, we propose to use the sSAPS with path loss compensation since it presents the best balance between complexity and performance.

E. Comparison between coherent and non-coherent schemes

In this subsection, we compare the NC and coherent approaches of the CF scheme, by means of a Monte Carlo simulation. We consider a multipath time-varying channel and implementation with orthogonal frequency division multiplexing (OFDM) modulation according to the 5G new radio numerology. The coherence time is calculated as $T_c = 0.15 f_D^{-1}$ [33], where f_D is the maximum Doppler frequency. The time correlation effects are implemented following the autocorrelation model of (2) in [34] and we assume the frequency offset (FO) of the LoS component is corrected with a FO correction. The OFDM symbol duration is $T_s = 1/\Delta_f$, where Δ_f is the subcarrier spacing of the OFDM. We define a ratio of coherence time to the OFDM symbol duration as $N_{CT} = T_c/T_s$, which is given in Table IV for 5G scenarios at the maximum foreseen speed of 500 km/h. Only values compatible with the allowed combinations of carrier frequency (f_c) and subcarrier spacing (Δ_f) in the 5G standard are shown; otherwise, they are marked with "-" in the table.

We consider a multipath channel with a delay spread of σ_τ < 1 microsecond so that the minimum coherence bandwidth is $B_c \approx 1/(5\sigma_\tau)$ = 200 kHz. The 5G standard [35] is followed with the pilot placing for the coherent scheme, where 4 out of 14 OFDM symbols correspond to pilots in each slot.

TABLE V
EXECUTION TIME COHERENT VERSUS NC.

Technique	Centr. MMSE	Proposed NC-CF
Exec. Time (ms)	918	34

In this configuration, $\tau = 10/14$ which affects the mean SNR for the coherent scheme by penalizing the BER as shown in (41). The AP configuration is the same as that of Section VI-B, and we only perform the All AP selection approach together with a path loss compensation in each AP to ensure a fair comparison between coherent and NC, since the AP selection is proposed for the NC scheme while one for the coherent is out of the scope of this work.

The reception process of the coherent scheme is composed of 3 steps, channel estimation, channel compensation and detection, while the NC scheme is composed of differential decoding and detection. We compare the coherent centralized MMSE and the NC-CF proposal of this manuscript. Regarding the complexity, and for reproducible purposes, the times shown here have been obtained for a single-thread AMD Ryzen 7 2700X 3.7 GHz general-purpose processor. The time shown in Table V is for one iteration of the reception process of each technique. It is clear from a complexity point of view that the proposed NC-CF is much more efficient than the coherent approach, mainly because pseudo-inverse calculations are avoided.

Fig. 5 shows the results for different N_{CT} values for 1 user for the coherent versus the NC scheme for a QPSK constellation. It can be seen that, for high SINR, the NC outperforms the coherent scheme except for $N_{CT} \geq 10$, since in this sense the channel is quasi-static and thus the coherent outperforms the NC. For $N_{CT} \leq 5$, the NC outperforms the coherent scheme for all SINR values, due to the fact that the NC is more robust against channel variability. Also, the NC outperforms the coherent counterpart in the low SINR regime even for large N_{CT}, due to the fact that NC avoids the channel estimation, which is largely erroneous for low SINR.

VII. CONCLUSIONS

In this chapter, we propose the combination of CF-mSIMO and NC processing, which solves some weaknesses of the single-cell NC and the coherent CF-mSIMO. We have first performed a theoretical analysis of the effect of Rician channels with spatial correlation on the SINR and SER of single user UL NC massive MIMO systems. We have then proposed several AP selection techniques for the proposed CF massive MIMO based on NC processing, to maximize the performance. These AP selection techniques are the BFS, the SAPS, the sSAPS and the "All AP". The BFS has the best performance and largest complexity, while the "All AP" has the smallest complexity. Later, we presented some characteristics and parameters to justify in which cases it makes sense to use NC over the coherent CF, depending on the channel estimation overhead, the delay and complexity of the detection and the performance comparison in fast varying and/or low SNR scenarios. Last, numerical results are provided to corroborate the theoretical analysis, to compare the time

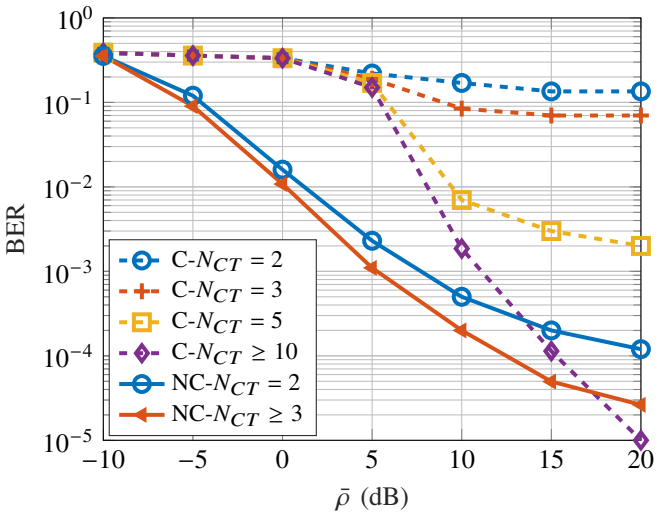

Fig. 5. Comparison between coherent centralized MMSE and NC for different N_{CT} values for 8 APs for the All AP selection approach for path loss compensation.

and performance of the AP selection techniques for different scenarios for the proposed CF NC massive MIMO and to compare the performance of the coherent and the NC CF for time varying channels. It is worth noting that the best AP selection approach for a low number of APs (the specific amount will be deployment dependent) and low SINR is the sSAPS without pathloss compensation, while for a very large number of APs or a high SINR the best is to select all the "visible" APs by the user with pathloss compensation. For the special case of single antenna APs, the All AP without pathloss compensation is the best option in the low SINR range, the sSAPS with pathloss compensation in the intermediate range, and the All AP the best in the high range.

This work contributes to the improvement of the performance of NC schemes combined with a CF processing approach. It has shown the viability of the proposed NC-CF and its advantages over a single cell processing and over its coherent counterpart. This is a significant improvement with respect to previous NC approaches in the literature and paves the way to achieving even better capabilities, particularly in scenarios where NC schemes are known to outperform coherent communications.

Appendix A
Mathematical Preliminaries

In section III, the properties of VG and Gamma distributions are used, which can be found in [21]–[23]:

- The product of two zero mean uncorrelated normal random variables X and Y with standard deviation σ_X and σ_Y respectively, follows a variance-gamma distribution with parameters $VG(1, 0, \sigma_X\sigma_Y, 0)$.
- The sum of R variables distributed according to $VG(k, 0, \sigma_i, 0)$ is distributed according to $VG\left(kR, 0, \sqrt{\frac{\sum_{i=1}^{R}\sigma_i^2}{R}}, 0\right)$.
- Scaling a $VG(1, 0, \sigma, 0)$ random variable by any parameter k results in a variable distributed as $VG(1, 0, k\sigma, 0)$.
- A distribution $VG(R, 0, \sigma, 0)$ with $R \to \infty$ can be regarded as a $\mathcal{N}(0, R\sigma^2)$.
- If a variable that follows a Gamma distribution $\Gamma(\delta, \beta)$ is scaled by a parameter k, the new variable is distributed as $\Gamma(\delta, k\beta)$.

The distribution of the sum of n independent Gamma variables $\Gamma(\delta_i, \beta_i)$ is approximated as a $\Gamma(\delta_m, \beta_m)$ with

$$\delta_m = \frac{\left(\sum_{i=0}^{n}\delta_i\beta_i\right)^2}{\sum_{i=0}^{n}\delta_i\beta_i^2}, \quad \text{and} \quad \beta_m = \frac{\sum_{i=0}^{n}\delta_i\beta_i^2}{\sum_{i=0}^{n}\delta_i\beta_i}, \tag{42}$$

and when $\delta_m >> \beta_m$ (true when there are several APs with small correlation), according to [36],

$$\Gamma(\delta_m, \beta_m) \approx \mathcal{N}\left(\delta_m\beta_m, \delta_m\beta_m^2\right) = \mathcal{N}\left(\sum_{i=0}^{n}\delta_i\beta_i, \sum_{i=0}^{n}\delta_i\beta_i^2\right). \tag{43}$$

Besides this, $\Re$ and $\Im$ are the real and imaginary parts of a random variable, and thus we can decompose the product of two complex variables as

$$(\Re_1 + j\Im_1)(\Re_2 + j\Im_2) = (\Re_1\Re_2 - \Im_1\Im_2) + j(\Re_1\Im_2 + \Im_1\Re_2), \tag{44}$$

composed of the sums and products of real normal variables, distributed according to

$$\Re_1\Re_2 - \Im_1\Im_2 \sim VG\left(2, 0, \sqrt{\frac{\sigma_{\Re_1}^2\sigma_{\Re_2}^2 + \sigma_{\Im_1}^2\sigma_{\Im_2}^2}{2}}, 0\right), \tag{45}$$

$$\Re_1\Im_2 + \Im_1\Re_2 \sim VG\left(2, 0, \sqrt{\frac{\sigma_{\Re_1}^2\sigma_{\Im_2}^2 + \sigma_{\Im_1}^2\sigma_{\Re_2}^2}{2}}, 0\right). \tag{46}$$

Appendix B
Distribution of the components of $\left[\mathbf{z}_a^n\right]_{r_a}$

Using the properties of VG and Gamma distributions, which can be found in [21]–[23], we have the distribution of each term:

$$\Re, \Im\left\{[\mathbf{z}_a]_{r_a}^{(2)}\right\} \sim VG\left(2, 0, \frac{\sigma_{\nu,a}^2}{2}, 0\right), \tag{47}$$

$$\Re, \Im\left\{[\mathbf{z}_a]_{r_a}^{(3,2)}, [\mathbf{z}_a]_{r_a}^{(4,2)}\right\} \sim VG\left(2, 0, \frac{\sqrt{\alpha_a}\sigma_{h,a}\sigma_{\nu,a}}{2}, 0\right), \tag{48}$$

$$[\mathbf{z}_a]_{r_a}^{(3,1)}, [\mathbf{z}_a]_{r_a}^{(4,1)} \sim \mathcal{CN}(0, \alpha_a|\bar{h}_a|^2\sigma_{\nu,a}^2), \tag{49}$$

$$\Re\left\{[\mathbf{z}_a]_{r_a}^{(1,1)}\right\} \sim \mathcal{N}(0, 2\alpha_a^2|\bar{h}_a|^2\sigma_{h,a}^2), \quad \Im\left\{[\mathbf{z}_a]_{r_a}^{(1,1)}\right\} = 0, \tag{50}$$

$$\Re\left\{[\mathbf{z}_a]_{r_a}^{(1,2)}\right\} \sim \Gamma(1, \alpha_a\sigma_{h,a}^2), \quad \Im\left\{[\mathbf{z}_a]_{r_a}^{(1,2)}\right\} = 0. \tag{51}$$

The summation of $2R_a$ elements for eq. (48) is given by

$$\sum_{r_a=1}^{R_a}\Re, \Im\left\{[\mathbf{z}_a]_{r_a}^{(3,2)} + [\mathbf{z}_a]_{r_a}^{(4,2)}\right\} \sim VG\left(4R_a, 0, \sqrt{\frac{\alpha_a\sigma_{\nu,a}^2}{4\sigma_{h,a}^{-2}}}, 0\right), \tag{52}$$

which in the limit $R_a \to \infty$ is distributed as

$$\sum_{r_a=1}^{R_a} \Re,\Im \left\{ [\mathbf{z}_a]_{r_a}^{(3,2)} + [\mathbf{z}_a]_{r_a}^{(4,2)} \right\} \overset{R_a \to \infty}{\sim} \mathcal{N}\left(0, R_a \alpha_a \sigma_{h,a}^2 \sigma_{\nu,a}^2\right). \tag{53}$$

Similar to (52) and (53) we can calculate the rest of the terms. It is worth noting that for (49) a total of $2R_a$ terms are summed, while R_a terms are summed for (47). As such,

$$\sum_{r_a=1}^{R_a} \Re,\Im \left\{ [\mathbf{z}_a]_{r_a}^{(3,1)} + [\mathbf{z}_a]_{r_a}^{(4,1)} \right\} \overset{R_a \to \infty}{\sim} \mathcal{N}(0, R_a \alpha_a |\bar{h}_a|^2 \sigma_{\nu,a}^2), \tag{54}$$

$$\sum_{r_a=1}^{R_a} \Re,\Im \left\{ [\mathbf{z}_a]_{r_a}^{(2)} \right\} \overset{R_a \to \infty}{\sim} \mathcal{N}\left(0, R_a \frac{\sigma_{\nu,a}^4}{2}\right). \tag{55}$$

In a certain AP whose antennas are spatially correlated, the summation of the R_a elements in the AP for eqs. (50) and (51) can be calculated following the properties found in [20], [36], [37] (these terms only contribute to the real part) as

$$\sum_{r_a=1}^{R_a} \Re \left\{ [\mathbf{z}_a]_{r_a}^{(1,1)} \right\} \overset{R_a \to \infty}{\sim} \mathcal{N}(0, 2\alpha_a^2 |\bar{h}_a|^2 \sigma_{h,a}^2 \mathbf{1}^T \mathbf{R}_a \mathbf{1}) \tag{56}$$

$$\sum_{r_a=1}^{R_a} \Re \left\{ [\mathbf{z}_a]_{r_a}^{(1,2)} \right\} \overset{R_a \to \infty}{\sim} \mathcal{N}\left(R_a \alpha_a \sigma_{h,a}^2, \alpha_a^2 \sigma_{h,a}^4 ||\mathbf{R}_a||_2^2\right). \tag{57}$$

Appendix C
P_s double integral to single integral

The double integral of (24) can be simplified by doing the following change of variables

$$a = \frac{\left(\sigma_\Re^2 - \sigma_\Im^2\right)\sin^2\gamma + \sigma_\Im^2}{2\sigma_\Re^2\sigma_\Im^2},\ b = \frac{2\sigma_\Im^2 \mu_\Re \cos\gamma}{2\sigma_\Re^2\sigma_\Im^2},\ c = \frac{\sigma_\Im^2 \mu_\Re^2}{2\sigma_\Re^2\sigma_\Im^2}, \tag{58}$$

and defining and solving the following integral

$$\int_0^\infty r e^{-\left(\frac{r\cos(\gamma)-\mu_\Re}{\sqrt{2}\sigma_\Re}\right)^2} e^{-\left(\frac{r\sin(\gamma)-\mu_\Im}{\sqrt{2}\sigma_\Im}\right)^2} dr = \int_0^\infty r e^{-ar^2+bx-c} dr = e^{-c} \frac{\sqrt{\pi} b e^{\frac{b^2}{4a}} \left(\operatorname{erfc}\left(\frac{b}{2\sqrt{a}}\right) + 1\right) + 2\sqrt{a}}{4a^{3/2}}, \tag{59}$$

so the double dimensional integral of (24) turns to the integral in (25).

References

[1] *5G end to end Key Performance Indicators (KPI)* , 3GPP Std. 28.554, 2021.

[2] W. Saad, M. Bennis, and M. Chen, "A Vision of 6G Wireless Systems: Applications, Trends, Technologies, and Open Research Problems," *IEEE Network*, vol. 34, no. 3, pp. 134–142, 2019.

[3] E. Björnson, J. Hoydis, and L. Sanguinetti, "Massive MIMO networks: Spectral, energy, and hardware efficiency," *Foundations and Trends® in Signal Processing*, vol. 11, no. 3-4, pp. 154–655, 2017. [Online]. Available: http://dx.doi.org/10.1561/2000000093

[4] M. J. Lopez-Morales, K. Chen-Hu, and A. Garcia-Armada, "Differential data-aided channel estimation for up-link massive SIMO-OFDM," *IEEE Open Journal of the Communications Society*, vol. 1, pp. 976–989, 2020.

[5] C. Tu and B. Champagne, "Subspace-based blind channel estimation for MIMO-OFDM systems with reduced time averaging," *IEEE Trans. Veh. Technol.*, vol. 59, no. 3, pp. 1539–1544, March 2010.

[6] A. G. Armada and L. Hanzo, "A Non-Coherent Multi-User Large Scale SIMO System Relaying on M-ary DPSK," in *2015 IEEE Intern. Conf. on Commun. (ICC)*, June 2015, pp. 2517–2522.

[7] K. Chen-Hu and A. G. Armada, "Non-Coherent Multiuser Massive MIMO-OFDM with Differential Modulation," in *2019 IEEE Intern. Conf. on Commun. (ICC)*, May 2019, pp. 1–6.

[8] J. Zhu, L. Xiao, P. Xiao, A. Quddus, C. He, and L. Lu, "Differential STBC-SM Scheme for Uplink Multi-User Massive MIMO Communications: System Design and Performance Analysis," *IEEE Trans. Veh. Technol.*, vol. 70, no. 10, pp. 10 236–10 251, 2021.

[9] A. Fazeli, H. H. Nguyen, H. D. Tuan, and H. V. Poor, "Non-Coherent Multi-Level Index Modulation," *IEEE Trans. Commun.*, vol. 70, no. 4, pp. 2240–2255, 2022.

[10] K.-H. Ngo, S. Yang, M. Guillaud, and A. Decurninge, "Joint Constellation Design for Noncoherent MIMO Multiple-Access Channels," *IEEE Trans. Inf. Theory*, vol. 68, no. 11, pp. 7281–7305, 2022.

[11] J. Zheng, J. Zhang, E. Björnson, and B. Ai, "Impact of channel aging on cell-free massive mimo over spatially correlated channels," *IEEE Trans. Wireless Commun.*, vol. 20, no. 10, pp. 6451–6466, 2021.

[12] M. J. L. Morales, K. Chen-Hu, and A. G. Armada, "Effect of Spatial Correlation on the Performance of Non-coherent Massive MIMO based on DMPSK," in *2021 IEEE Global Commun. Conf. (GLOBECOM)*, 2021, pp. 1–6.

[13] K. Chen-Hu, Y. Liu, and A. G. Armada, "Non-Coherent Massive MIMO-OFDM Down-Link Based on Differential Modulation," *IEEE Trans. Veh. Technol.*, vol. 69, no. 10, pp. 11 281–11 294, 2020.

[14] L. Sanguinetti, E. Björnson, and J. Hoydis, "Toward Massive MIMO 2.0: Understanding Spatial Correlation, Interference Suppression, and Pilot Contamination," *IEEE Trans. Commun.*, vol. 68, no. 1, pp. 232–257, 2020.

[15] C. He and R. D. Gitlin, "Limiting performance of massive MIMO downlink cellular systems," in *2016 Information Theory and Applications Workshop (ITA)*, 2016, pp. 1–6.

[16] H. Q. Ngo, A. Ashikhmin, H. Yang, E. G. Larsson, and T. L. Marzetta, "Cell-Free Massive MIMO Versus Small Cells," *IEEE Trans. Wireless Commun.*, vol. 16, no. 3, pp. 1834–1850, 2017.

[17] W. Mennerich and W. Zirwas, "User Centric Coordinated Multi Point Transmission," in *2010 IEEE 72nd Veh. Tech. Conf. - Fall*, 2010, pp. 1–5.

[18] H. Q. Ngo, A. Ashikhmin, H. Yang, E. G. Larsson, and T. L. Marzetta, "Cell-free massive MIMO versus small cells," *IEEE Trans. Wireless Commun.*, vol. 16, no. 3, pp. 1834–1850, 2017.

[19] H. Jafarkhani, *Space-time coding: theory and practice*. Cambridge university press, 2005.

[20] R. A. Johnson, D. W. Wichern *et al.*, *Applied multivariate statistical analysis*. Prentice hall Upper Saddle River, NJ, 2002, vol. 5, no. 8.

[21] R. Gaunt, "Variance-gamma approximation via stein's method," *Electron. J. Probab.*, vol. 19, p. 33 pp., 2014. [Online]. Available: https://doi.org/10.1214/EJP.v19-3020

[22] R. E. Gaunt, "A note on the distribution of the product of zero mean correlated normal random variables," 2018.

[23] S. Covo, A. Elalouf *et al.*, "A novel single-gamma approximation to the sum of independent gamma variables, and a generalization to infinitely divisible distributions," *Electronic Journal of Statistics*, vol. 8, no. 1, pp. 894–926, 2014.

[24] Proakis, *Digital Communications 5th Edition*. McGraw Hill, 2007.

[25] A. A. Polegre, F. Riera-Palou, G. Femenias, and A. G. Armada, "Channel Hardening in Cell-Free and User-Centric Massive MIMO Networks With Spatially Correlated Ricean Fading," *IEEE Access*, vol. 8, pp. 139 827–139 845, 2020.

[26] M. Shamaiah, S. Banerjee, and H. Vikalo, "Greedy sensor selection: Leveraging submodularity," in *49th IEEE conf. on dec. and cont. (CDC)*. IEEE, 2010, pp. 2572–2577.

[27] A. Alkhateeb and R. W. Heath, "Frequency Selective Hybrid Precoding for Limited Feedback Millimeter Wave Systems," *IEEE Trans. Commun.*, vol. 64, no. 5, pp. 1801–1818, May 2016.

[28] E. Björnson and L. Sanguinetti, "Making Cell-Free Massive MIMO Competitive With MMSE Processing and Centralized Implementation," *IEEE Trans. Wireless Commun.*, vol. 19, no. 1, pp. 77–90, 2020.

[29] S. M. Kay, *Fundamentals of Statistical Signal Processing: Estimation Theory*. USA: Prentice-Hall, Inc., 1993.

[30] E. Björnson and L. Sanguinetti, "Scalable Cell-Free Massive MIMO Systems," *IEEE Trans. Commun.*, vol. 68, no. 7, pp. 4247–4261, 2020.

[31] D. Mi, M. Dianati, L. Zhang, S. Muhaidat, and R. Tafazolli, "Massive mimo performance with imperfect channel reciprocity and channel estimation error," *IEEE Trans. Commun.*, vol. 65, no. 9, pp. 3734–3749, 2017.
[32] Technical Specification Group, "Study on 3D channel model for LTE," 3GPP, Tech. Rep. 36.873 V12.0.0 Release 12, 2014.
[33] T. S. Rappaport *et al.*, *Wireless communications: principles and practice*. Prentice Hall PTR, 1996, vol. 2.
[34] K. E. Baddour and N. C. Beaulieu, "Autoregressive modeling for fading channel simulation," *IEEE Trans. Wireless Commun.*, vol. 4, no. 4, pp. 1650–1662, July 2005.
[35] *Physical Channels and Modulation (Release 15)*, 3GPP Std. 38.211, 2018.
[36] L. M. Leemis and J. T. McQueston, "Univariate distribution relationships," *The American Statistician*, vol. 62, no. 1, pp. 45–53, 2008.
[37] Y. Feng, M. Wen, J. Zhang, F. Ji, and G. Ning, "Sum of arbitrarily correlated gamma random variables with unequal parameters and its application in wireless communications," in *2016 Intern. Conf. on Computing, Networking and Communications (ICNC)*, 2016, pp. 1–5.

Manuel J. Lopez-Morales (S'19-GS'23) received the B.Eng. degree (Hons.) in Electrical Engineering from the Polytechnic University of Madrid in 2015, a double M.Sc. degree (Hons.) in Telecommunications Engineering and Wireless Communications from the Polytechnic University of Madrid and Lund University, in 2018 and the PhD degree (SCL) from the Universidad Carlos III de Madrid in 2023. He has several international experiences in Italy, Japan, Sweden, France and Portugal. His research interests include signal processing, wireless communications, antenna technology, massive MIMO, machine learning, and optimization applied to communications.

Kun Chen-Hu (S'16-GS'20-M'21) received his Ph.D. degree in Multimedia and Communications in 2019 from Universidad Carlos III de Madrid (Spain). He has worked as a post-doctoral researcher in the same institution for 3 years. Currently, he is a researcher at Aalborg University (Denmark). He was awarded by UC3M in 2019 recognizing his outstanding professional career after graduation. He visited Eurecom (France), Vodafone Chair TU Dresden (Germany) and other research institutions as a guest researcher. He also participated in different research projects in collaboration with several top companies in the area of mobile communications. He was the Web Chair for Globecom 2021 and Meditcom 2024, Madrid (Spain), and online content editor for IEEE ComSoc. He was awarded as Exemplary Reviewer by IEEE Trans. on Communications in 2019 and 2020, and IEEE Communications Letters in 2019. His research interests are related to signal processing techniques, such as waveforms design, reconfigurable intelligent surfaces, non-coherent massive MIMO and channel estimation.

Alberto Alvarez-Polegre (S'18-M'22) received the M.Sc. degree in telecommunications engineering from the University of Las Palmas de Gran Canaria, Spain, in 2015, and the Ph.D. degree in multimedia and communications from the University Carlos III de Madrid, Spain, in 2021. From 2015 to 2017, he was with GMV as a software engineer for aircraft communications development and testing. From 2015 to 2021 he was a predoctoral fellow with the Communications Research Group at the University Carlos III de Madrid where he was part of the OPALL5G (Small Cells Performance Optimization in 5G NR Networks) project jointly developed with Nokia Spain. Since 2021 he has been an academic customer success engineer and wireless communications specialist at The MathWorks.

Ana García Armada (S'96-A'98-M'00-SM'08) received the Ph.D. degree in electrical engineering from the Polytechnical University of Madrid in February 1998. She is currently a Professor at Universidad Carlos III de Madrid, Spain. She is leading the Communications Research Group at this university. She is leading the Communications Research Group at this university. She has been visiting scholar at Stanford University, Bell Labs and University of Southampton. She has participated and coordinated a large number national and international research projects as well as contracts with the industry, all of them related to wireless communications. Her research has resulted in 9 book chapters, and more than 250 publications in prestigious international journals and conferences, as well as 5 patents. She has contributed to international standards organizations, such as ITU and ETSI, she is a member of the expert group of NetworldEurope European Technology Platform and was Vice-Chair of the advisory committee 5JAC of the ESA as expert appointed by Spain on 5G (2019-2023). She has been Editor (2016–2019, Exemplary Editor Award 2017 and 2018) and Area Editor (2019-2020, Exemplary Editor Award 2020) of IEEE Communication Letters. She is an Editor of IEEE Transactions on Communications since 2019, Area Editor of IEEE Open Journal of the Communications Society since 2019, Editor of the ITU Journal on Future and Evolving Technologies and is a regular member of the technical program committees of the most relevant international conferences in his field. She has formed / is part of the organizing committee of the IEEE MeditCom 2024 (General Chair), IEEE MeditCom 2023, IEEE WNCN 2024, IEEE Globecom 2022, IEEE Globecom 2021 (General Chair), IEEE Globecom 2019IEEE Vehicular Technology Conference Spring 2018, 2019 and Fall 2018, among others. She is Vice Chair of the IEEE ComSoc Signal Processing and Computing for Communications Committee, has been Secretary and Chair of the IEEE ComSoc Women in Communications Engineering Standing Committee. She has been a Member at Large of the Board of Governors, Director of Online Content and member of several management committees in the IEEE Communications Society, where she is now the VP of Member and Global Activities. She has received the Young Researchers Excellence Award, the Award to Outstanding achievement in research, teaching and management and the Award to Best Practices in Teaching, all from University Carlos III of Madrid. She was awarded the third place Bell Labs Prize 2014 for shaping the future of information and communications technology. She received the Outstanding service award from the IEEE ComSoc Signal Processing and Communications Electronics technical committee in 2019 and the Outstanding service award from the IEEE ComSoc Women in Communications Engineering Standing Committee in 2020. She received the IEEE ComSoc/KICS Exemplary Global Service Award in 2022. Her main research interests are signal processing techniques applied to wireless communications.